



Original Paper

# Pore–Fracture Structure Characteristics of Low-Medium Rank Coals from Eastern Surat Basin by FE-SEM and NMR Experiments

Zehong Cui,<sup>1</sup> Zheng Zhang,<sup>2,3</sup> Wensong Huang,<sup>1</sup> Lingli Liu,<sup>1</sup> Jianjun Wang,<sup>1</sup> Xiaoyi Wei,<sup>1</sup> and Jian Shen<sup>2</sup>

Received 8 October 2023; accepted 27 December 2023  
Published online: 5 February 2024

The Middle Jurassic Walloon Subgroup coals in Australia's Surat Basin are extremely rich in low-medium rank coal seam gas (CSG) resources, making it one of the world's most productive CSG development basins. The desorption, diffusion and seepage behaviors of CSG are remarkably influenced by the pore–fracture structure characteristics of coals; therefore, their detailed characterizations are greatly significant for CSG exploration and development. There are, however, currently few researches on the pore–fracture structure characteristics of Surat Basin coals. Thus, 12 low-medium rank coals ( $R_r$ : 0.42–0.60%) from the Walloon subgroup of Eastern Surat Basin were obtained for this study, and then coal petrology analyses, field emission scanning electron microscopy and nuclear magnetic resonance (NMR) experiments were performed on these samples. The results show that the organic macerals of Surat coals are dominated by vitrinite, followed by liptinite, and the inertinite is generally rare. The average porosity, movable porosity and movable water saturation of the coal samples were 5.08%, 1.01% and 22.47%, respectively. The coal samples' pore–fracture structure was characterized by an overwhelming predominance of MIT (micropores and transition pore) and relatively less developed ME (mesopore) and MAF (macropore and fracture), with average volume proportions of 74.58%, 14.06% and 11.36%, respectively. The movable porosities of different pore–fracture structure types were obtained, and the average values were presented as MAF > ME > MIT. The NMR experiments showed that the average movable spaces in the MIT, ME and MAF of the coal samples were 6.6%, 41.8% and 97.9%, respectively. The pore–fracture structure of the sampled coals was influenced by coal maturity, as well as the coal macerals. The coal facies have some impacts on the porosities of coal samples, and the coals with higher texture preservation index and vegetation index, and lower gelation index overall have higher porosities.

**KEY WORDS:** Coal seam gas, Pore–fracture structure, Low-medium rank coal, Nuclear magnetic resonance, Surat Basin.

## INTRODUCTION

Coal seam gas (CSG), generated during coal-forming processes and mainly composed of methane (Montgomery 1999; Xu et al. 2022), is a significantly important kind of unconventional gas resource

<sup>1</sup>PetroChina Research Institute of Petroleum Exploration and Development, Beijing 10080, China.

<sup>2</sup>School of Resources and Geosciences, China University of Mining and Technology, Xuzhou 221116, China.

<sup>3</sup>To whom correspondence should be addressed; e-mail: zzcumt@cumt.edu.cn

(Moore 2012; Salmachi et al. 2021). Many nations that produce coal, like the USA, Australia, Canada, China and so on, have favored CSG (Qin et al. 2018; Zou et al. 2019; Mohamed and Mehana 2020) as a sort of clean and highly efficient energy (Zhao et al. 2020) as well as an important chemical material (Li et al. 2023). The low-medium (mean random vitrinite reflectance,  $\bar{R}_r < 2.0\%$ ) rank (ISO 11706 2005) CSG is widespread in the world and has been quite successful in the Powder River Basin of America (Ayers Jr 2002), the Alberta Basin of Canada (Mastalerz and Drobniak 2020) and the Surat Basin of Australia (Salmachi et al. 2021).

The Surat Basin's Walloon Subgroup coals host a world-class, low-medium (mainly low rank,  $R_r < 0.5\%$ ) rank CSG performance (Hamilton et al. 2015; Mukherjee et al. 2020). The Surat Basin had  $8507 \times 10^8 \text{ m}^3$  of proven and probable (2P) CSG resources as of the end of 2017 (Queensland Government 2018), and it produced approximately  $300 \times 10^8 \text{ m}^3$  of CSG in 2018. This accounts for over 75% of Australia's total CSG production (Queensland Government 2019), making the Surat Basin an important base for the liquefied natural gas production in eastern Australia (DNRM 2016; Salmachi et al. 2021).

The CSG existing in a coal reservoir will be produced through desorption, diffusion and seepage processes, which all occur in the coal reservoir's pore-fracture system, once the reservoir pressure drops below the desorption pressure (Mukherjee et al. 2020; Luo et al. 2021). Thus, the development scale and structural characteristics of pore-fracture determine the gas desorption and diffusion behaviors, as well as coal permeability, and then affect the CSG production performances (Ouyang et al. 2016; Liu et al. 2023). Therefore, characterizations of the pore-fracture structure of coal reservoirs are greatly significant for CSG exploration and development. However, to date, few researches on the Surat Basin coals' pore-fracture structure characteristics have been undertaken.

The pore-fracture structure of coals is very complex and its heterogeneity is extremely strong (Wang et al. 2019; Liu et al. 2023). The pore-fracture structure of coals has been classified using a variety of methods (Hodot 1966; Thommes et al. 2015; Cheng and Hu 2023), and the most commonly used method is to divide pore-fracture structure into micropores, transition pores, mesopores, macropores and fractures according to the mechanical

properties of coals and gas adsorbent and permeable properties in coals (Hodot 1966). Further classifying pores and fractures of coals into adsorption and seepage pores was performed by Yao et al. (2008, 2009). Adsorption pores (diameter  $< 100 \text{ nm}$ ), composed of micropores ( $< 10 \text{ nm}$ ) and transition pores ( $10\text{--}100 \text{ nm}$ ), have extremely low permeability and mainly control gas adsorption, desorption, and diffusion behaviors in coals (Zhao et al. 2016a, 2016b). The seepage pores (diameter  $> 100 \text{ nm}$ ) including mesopores ( $100\text{--}1000 \text{ nm}$ ), macropores ( $> 1000 \text{ nm}$ ) and fractures play a crucial role in coal permeability and mainly provide flow paths for fluids in coals (Zhang et al. 2020).

Numerous techniques have been utilized to analyze coal pore-fracture structure. In summary, there are three categories: photoelectric radiation, fluid immersion and digital core techniques. The common photoelectric radiation methods include field emission scanning electron microscopy (FE-SEM) (Li et al. 2023), nuclear magnetic resonance (NMR) (Yao et al. 2010a; 2010b), atomic force microscope (AFM) (Li et al. 2020), high-resolution transmission electron microscopy (HRTEM) (Zhao et al. 2014), etc. Mercury intrusion porosimetry (Guo et al. 2019), low-temperature nitrogen adsorption (Nie et al. 2015) and  $\text{CO}_2$  adsorption (Hou et al. 2017) are commonly utilized fluid immersion techniques. The common digital core technique for coals' pore-fracture structure study is micro-computed tomography (Micro-CT) (Ramandi et al. 2016; Li et al. 2017b). Every method has its advantages and disadvantages in characterizing the pore-fracture structure of coals. The NMR has been utilized widely in recent years to study the coals' pore-fracture structure not only because of its non-destructive and rapid testing characteristics, but also because it can detect the movable porosity of coals (Yao et al. 2010a; Li et al. 2023). The movable porosity refers to the porosity of linked pore-fractures in coal that facilitates the flow of movable fluids, and it is greatly crucial for coal permeability (Yao et al. 2010b; Zhang et al. 2018; Zheng et al. 2018). Thus, determination of movable porosity is one of the key indicators to evaluate coal permeability (Yao et al. 2010a).

In this study, coal petrology analyses, FE-SEM and NMR experiments were performed on 12 Eastern Surat Basin coal samples. The pore-fracture structure characteristics of these samples were investigated. In addition, the porosities and movable porosities of different pore-fracture structure types

were determined. Finally, the influences of coal maturity, macerals and coal-forming environments on the pore–fracture development characteristics of coals were discussed. The findings in this work are expected to provide suggestions for the CSG exploration and development in the Eastern Surat Basin.

## GEOLOGICAL SETTINGS

The Surat Basin, located in eastern Australia, is a large Mesozoic intracratonic basin and covers an area of approximately  $30 \times 10^4 \text{ km}^2$  (Andrade et al. 2023) (Fig. 1a). The Surat Basin is relatively simple in structure and composed of three structural units: the eastern slope zone, the western slope zone, and the central depression zone (Fig. 1b). The study area in this work is mainly in the eastern slope zone. Two nose structures, namely Undulla and Kogan, exist in this area (Fig. 1c). Besides, some faults with a major strike of NE–SW, NW–SE or nearly N–S develop in the research region (Fig. 1c). The strata of the study area overall dip to the southwest, with angles of less than  $5^\circ$  (Fig. 1c).

The Walloon Subgroup (Fig. 2) in Middle Jurassic is a set of coal-bearing strata, with a typical thickness of 300–500 m (Morris and Martin, 2016). The Walloon Subgroup is composed mainly of mudstone, siltstone, sand and coal (Fig. 2), which were deposited in a fluvio–lacustrine environment (Shields and Esterle 2015). The coals, which have poor lateral continuity and large thickness variation, were mostly the product of a meandering river's flood plain swamp. The Walloon Subgroup contains two coal measures, i.e., Juandah and Taroom, and they are separated by the Tangalooma Sandstone (Fig. 2).

The Walloon Subgroup generally contains more than 50 individual coal seams with thicknesses varying from stringer-scale to 3–4 m, and the cumulative thickness can reach 50 m (Hamilton et al. 2014b); the majority of the coal seams are thin ( $< 1 \text{ m}$ ), discontinuous and hard to correlate over large distances (Martin et al. 2013). Coal seams mainly occur in the Juandah and Taroom Coal Measures; in addition, the Tangalooma Sandstone Formation and Eurombah Formation may also include minor coal seams. The coal seams in the Juandah and Taroom coal measures in this work were divided into six coal groups according to previous studies on the stratigraphic framework (Scott

et al. 2004; Hamilton et al. 2014a; Cui et al. 2022): Kogan, Macalister, Wambo, Argyle, Upper Taroom and Condamine (Fig. 2).

## SAMPLES AND EXPERIMENTS

### Sample Collection

The experimental coal samples were collected from drilling cores of eight CSG Wells in the Eastern Surat Basin (Fig. 1). In total, 12 coal samples (Table 1) were collected, covering five coal groups, including Macalister, Wambo, Argyle, Upper Taroom and Eurombah Formation. The mid-depth of the samples ranged 120.75–565.09 m. In this study, coal petrology analysis (vitrinite reflectance measurement and macerals quantification), FE-SEM, and NMR experiments were carried out on the coal samples.

### Coal Petrology Analyses

The fragmental coal samples were crushed and sieved into 20–40 mesh, and dried at  $70^\circ \text{C}$  for 48 h in a drying oven, after which the crushed samples were made into pulverized coal polished sections, respectively. On a LeitzMPV-3 photometer microscope, quantitative analyses of macerals and measurements of vitrinite reflectance were carried out by ISO7404.3-1994 (1994) and ISO7404.5-1994 (1994) standards, respectively.

### FE-SEM Experiments

Before FE-SEM experiments, Ar ion polishing was performed on each block sample with size of approximately  $10 \text{ mm} \times 10 \text{ mm} \times 20 \text{ mm}$  to ensure a smooth surface. The samples were then dried at  $70^\circ \text{C}$  for 48 h in a drying oven. After that, the pores and fractures in the coals were observed on a FE-SEM instrument produced by Zeiss of Germany at  $24^\circ \text{C}$  and relative humidity of 35%.

### NMR Experiments

Based on the NMR relaxation theory, the transverse relaxation time ( $T_2$ ) in the porous media

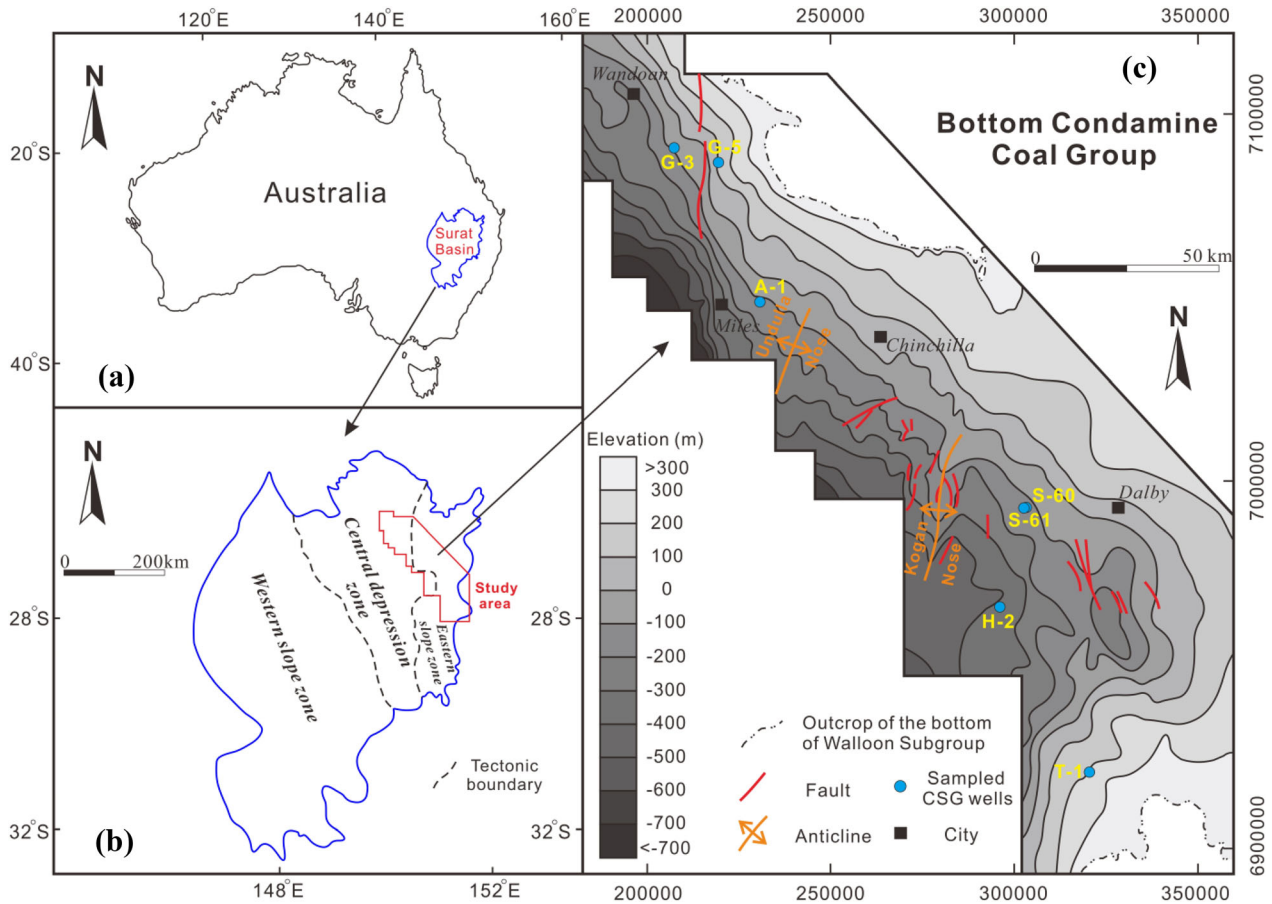


**Figure 1.** (a) Location of Surat Basin in Australia. (b) Location of the study area in the Surat Basin. (c) Elevation contours of the bottom of Condamine Coal Group and the location of sampled CSG wells.

of rock can be expressed as (Kenyon et al. 1988; Howard et al. 1993):

$$\frac{1}{T_2} = \frac{1}{T_{2B}} + \frac{1}{T_{2S}} \quad (1)$$

$$\frac{1}{T_{2S}} = \rho_2 \left( \frac{S}{V} \right) \quad (2)$$

where  $T_{2B}$  represents bulk relaxation time;  $T_{2S}$ , surface relaxation time;  $\rho_2$ , surface relaxation strength, which is a constant; and  $S/V$  is the ratio of the surface area to the volume.

The signal peak of bulk relaxation appears at a long relaxation time, generally greater than 3 s, whereas the surface relaxation appears rapidly and is generally measured in millisecond (Coates et al. 1999; Sun et al. 2018). Thus, the  $1/T_{2B}$ , the first term

on the right of Eq. 1, can be negligible. Thereby, Eq. 1 can be simplified as:

$$\frac{1}{T_2} = \frac{1}{T_{2S}} = \rho_2 \left( \frac{S}{V} \right) \quad (3)$$

The  $T_2$  of the rock is proportional to the pore radius, as shown by Eq. 3. Thus, the  $T_2$  can be used as a measure of pore size. The greater the pore size, the higher the  $T_2$  value, and vice versa. This is the theoretical basis for the analysis of pore size distribution of rock by the NMR  $T_2$  spectrum.

Because NMR only measures the number of  $^1\text{H}$  atoms in a sample of rock, the amount of water in the pore–fracture is proportional to the cumulative amplitude (CA) of the  $T_2$  spectrum (Sun et al. 2018). Therefore, in this experiment, the amplitude index A, which represents the ratio of the water volume in the coal to the CA of the  $T_2$  spectrum, was used to

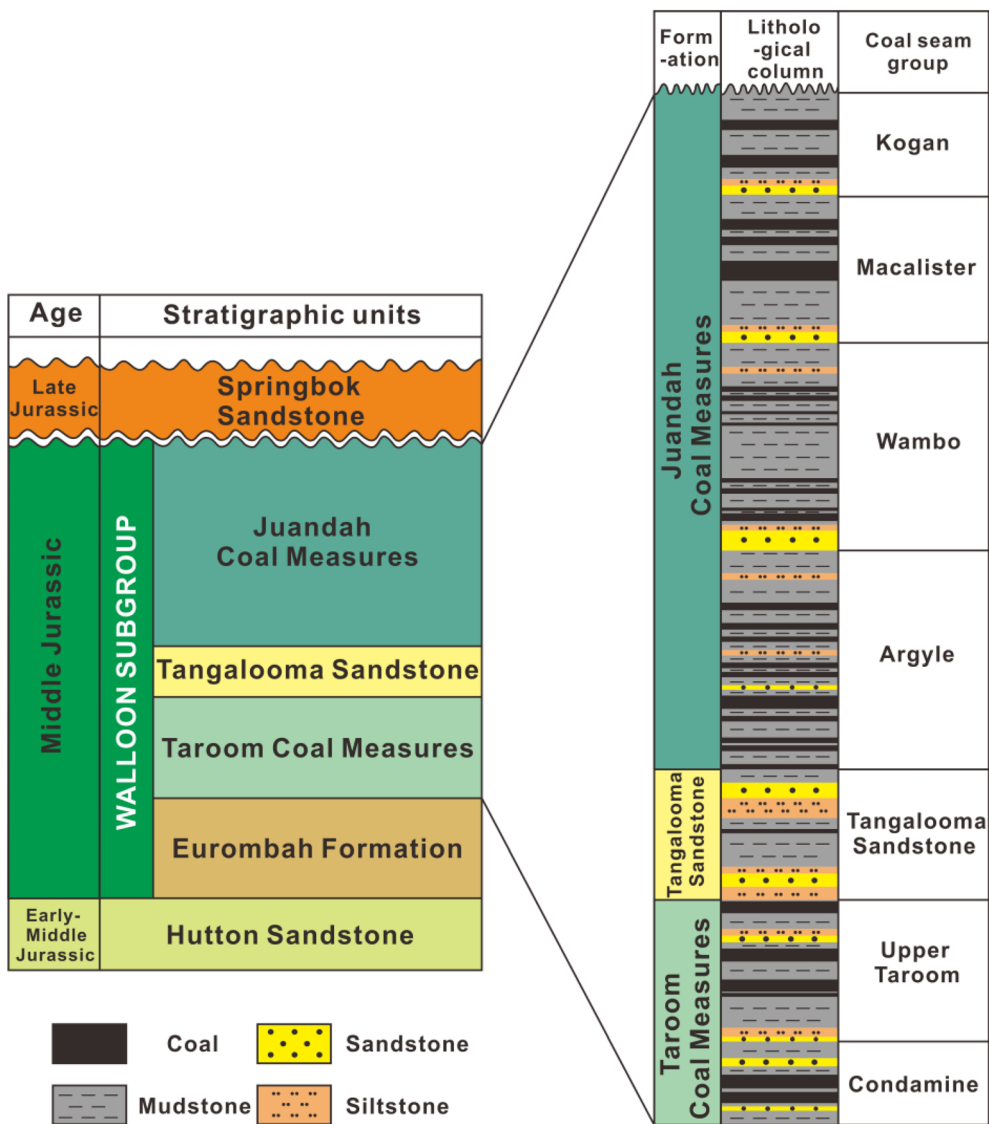


**Figure 2.** Comprehensive stratigraphic column of Taroom–Juandah coal measures of Walloon Subgroup in the study area.

**Table 1.** Basic information of coal samples collected from Eastern Surat Basin

Well name	Sample I.D.	Mid-depth (m)	Coal group	Well name	Sample I.D.	Mid-depth (m)	Coal group	
H-2	Su-1	459.30	Macalister	S-60	Su-7	309.40	Upper Taroom	
	Su-2	514.03	Wambo		Su-8	120.75	Macalister	
	Su-3	514.16	Wambo		A-1	Su-9	157.60	Macalister
	Su-4	565.09	Argyle		G-5	Su-10	182.65	Upper Taroom
S-60	Su-5	249.40	Argyle	T-1	Su-11	237.20	Eurombah F.M.	
	Su-6	249.70	Argyle	G-3	Su-12	270.40	Upper Taroom	

quantify the water volume in the coal. In this work, the  $A$  value was obtained by measuring the CA and the mass of water in coal in six sets of NMR experiments. It can be seen in Figure 3 that the water volumes in the coal sample had excellent linear positive correlations with the CA of the  $T_2$  spectrum ( $R^2 = 0.9988$ ). From the slope of the fitted linear equation,  $A$  is determined to be 22765.

The NMR experiments in this work were carried out using a low-field NMR instrument called the RecCore-3000 (2.38 MHz), and the measuring accuracy was 3%. The related parameters were set as follows: wait time, 5 s; number of scans, 64; echo number, 2048; echo time, 0.6 ms; magnetic field strength, 1200 Gauss; experimental temperature, 30 °C.

In this study, three series of NMR experiments on conditions of dryness, fully saturated water ( $S_f$ ) and irreducible water ( $S_{ir}$ ) were performed on the coal samples. The experimental steps were as follows: (1) Dry the coal samples at 70 °C for 24 h in a drying oven, and then vacuumed for 8 h. After that, the NMR experiments were carried out on the vacuum-dried samples to obtain the  $T_2$  spectrum under the dry condition, namely the base  $T_2$  spectrums ( $T_{2b}$ ) of the coal samples. (2) Fully saturate the vacuum-dried samples with distilled water using a vacuum pressurization saturation system with maximum pressure of 10 MPa. The samples were weighed every two hours, and when the weights of the samples were constant, the samples were con-

sidered to be fully saturated. Then, the NMR experiments were carried out on the  $S_f$  samples to obtain the corresponding  $T_2$  spectrums ( $T_{2f}'$ ). (3) Remove the base  $T_2$  spectrum ( $T_{2b}$ ) from the  $T_{2f}'$ , and then the  $T_2$  spectrum ( $T_{2f}$ ) of the sample under the  $S_f$  condition was obtained. (4) Put the  $S_f$  coal samples into a centrifuge and centrifuged at a pressure of 2.65 MPa for 1.5 h at a high speed to obtain the  $S_{ir}$  coal samples. (5) Perform NMR experiments on the  $S_{ir}$  coal samples to obtain the corresponding  $T_2$  spectrums ( $T_{2i}'$ ). (6) Remove the base  $T_2$  spectrum ( $T_{2b}$ ) from the  $T_{2i}'$ , and then the  $T_2$  spectrum ( $T_{2i}$ ) of the sample under the  $S_{ir}$  condition was obtained.

## RESULTS

### Coal Property

From the coal petrology analyses (Table 2), the mean random vitrinite reflectance ( $\bar{R}_r$ ) of the 12 coal samples from Eastern Surat Basin ranged 0.42–0.60% (avg. 0.52%), indicating that the coals were subbituminous coal to high-volatile bituminous coal D in coal rank based on ISO 11706 (2005). The  $\bar{R}_r$  of the coal samples overall rose with burial depth, with correlation coefficient  $R$  of 0.45 (Fig. 4).

The organic macerals (on a whole-coal basis) (Table 2) were dominated by vitrinite, with contents ranging 66.6–82.2% (avg. 72.4%). The major vitrinite was collodetrinite (52.2–67.8%, avg. 59.1%) (Fig. 5a), followed by gelocollinite (2.2–10.6%, avg. 6.67%) (Fig. 5b) and corpogelinite (0–16.4%, avg. 4.87%) (Fig. 5b, c). Liptinite was the secondary maceral, accounting for 16.4–29.0%, with average content of 24.2%. The suberinite (6.8–14.0%, avg. 10.15%) (Fig. 5b, e, g) and resinite (4.2–12.2%, avg. 7.18%) (Fig. 5d, e) constituted the major liptinite, and sporinite (1.8–4.6%, avg. 3.3%) (Fig. 5e) and cutinite (1.8–3.8%, avg. 2.97%) (Fig. 5d, f, g) were the subordinate liptinite. The inertinite was generally rare and observed only in five coal samples, and it constituted approximately 1% of the overall composition on average. Among the sampled coals, only Su-9 had a relatively higher inertinite with value of 11.2% (Table 2). The inertinite that can be detected in the coal samples include fusinite (Fig. 5h), semifusinite (Fig. 5i), inertodetrinite (Fig. 5i) and macrinite (Fig. 5i). The mineral content

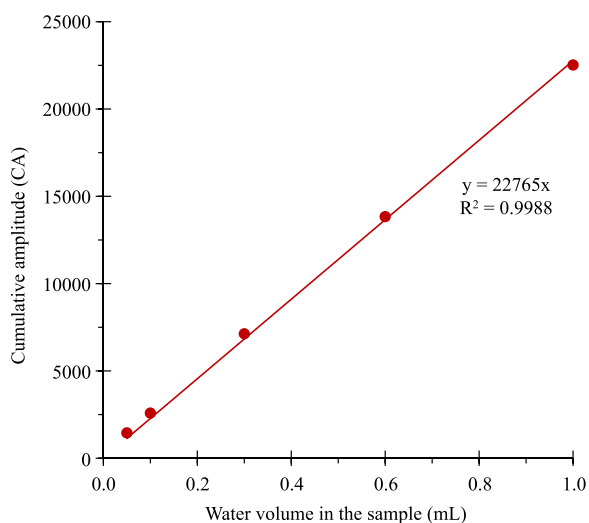


**Figure 3.** Relationship between water volume in the coal sample and the cumulative amplitude of  $T_2$  spectrum in the NMR experiments.

Table 2. Petrographic composition (vol.%, on whole-coal basis) of coals from Eastern Surat Basin

Sample I.D.	Rr (%)	Vitrinite group (%)										Inertinite group (%)										Liptinite group (%)										Mineral (%)	
		T	Ct	Vi	Cg	Cd	Ge	ΣV	F	Sf	Ma	Mi	ID	Fg	Sec	ΣI	Sp	Cu	Re	Sub	Bar	Al	Ful	Bit	Ex	Lip	ΣL	ΣM					
Su-1	0.42	0	0.4	0	0	61.2	10.6	72.2	0	0	0	0	0	0	0	2.6	3.0	12.2	8.4	0	0	0	0	0	0.2	0	26.4	1.4					
Su-2	0.55	0	3.4	0	2.4	62.8	4.4	73.0	0	0	0	0	0	0	0	4.6	3.0	4.8	10.2	0	0	0	0	0	0	0	22.6	4.4					
Su-3	0.56	0	1.0	0	0	67.8	7.4	76.2	0	0	0	0	0	0	0	4.2	3.8	6.2	8.4	0	0	0	0	0	0.2	0	22.8	1.0					
Su-4	0.60	0	1.6	0	8.2	61.0	2.2	73.0	0.2	0	0	0.2	0	0	0.4	3.4	2.4	5.4	10.4	0	0	0	0	0	2.0	0	23.6	3.0					
Su-5	0.56	2.2	0	0	16.4	57.2	4.2	82.2	0	0	0	0	0	0	0	1.8	2.2	4.2	6.8	0	0	0	0	0	1.4	0	16.4	1.4					
Su-6	0.56	0.4	0	0	3.4	55.8	10.6	70.6	0.2	0	0	0	0	0	0.2	4.6	3.8	6.2	13.6	0	0	0	0	0	0.6	0	28.8	0.8					
Su-7	0.54	0.4	0	0	3.6	53.6	9.8	67.8	0.6	0	0	0	0	0	0.6	4.2	3.8	6.6	14	0	0	0	0	0	0.4	0	29.0	2.6					
Su-8	0.45	0	0	0	6.4	56.4	6.6	69.4	0.8	0	0	0	0	0	0.8	4.2	3.4	8.4	10.6	0	0	0	0	0	0.6	0	27.2	2.6					
Su-9	0.44	0	1.4	0	2.2	58.8	4.2	66.6	2.2	4.6	1.8	0	2.6	0	11.2	3.4	1.8	7.8	8.4	0	0	0	0	0	0.2	0	21.6	0.6					
Su-10	0.48	0	2.6	0	5.6	63.8	6.2	78.2	0	0	0	0	0	0	2	2.6	4.4	9.4	0	0	0	0	0	0	0	18.4	3.4						
Su-11	0.45	0	2	0	4.4	59	6.4	71.8	0	0	0	0	0	0	2.4	3.2	8.4	9.8	0	0	0	0	0	1	0	24.8	3.4						
Su-12	0.59	0	2.2	0	5.8	52.2	7.4	67.6	0	0	0	0	0	0	2.2	2.6	11.6	11.8	0	0	0	0	0	0	0	28.2	4.2						

Rr mean random vitrinite reflectance = %, T telinite, Ct collotelinite, Vi vitrodetrinite, Cg coropogelinite, Cd collodetrinite, Ge gelocollinite, V vitrinite group, F fusinite, Sf semifusinite, Ma macrinite, Mi micronite, ID inertodetrinite, Fg funginite, Sec secretinite, I inertinite group, Sp sporinite, Cu cutinite, Re resinite, Sub suberinite, Bar barkinite, Al alginite, Ful fluorophor, Bit bituminite, Ex exsudatinite, Lip liptodetrinite, L liptinite group, M mineral

in the tested coal samples ranged 0.4–4.4%, averaging 2.4%.

Pores and Fractures Observed By FE-SEM

The FE-SEM is a common and the most visualized tool to observe the pores and fractures in coals. In this work, by using the FE-SEM technology, the pores and fractures of sampled Eastern Surat Basin coals were observed. It was found that the pore shapes in the coal samples were various, and there are circle, subcircular, oval, slit and so on, and among them, subcircular and oval shape pores were dominant. Macropores, mesopores, transition pores and micropores were all observed in the coal samples (Fig. 6). The distribution of macropores was relatively dispersedly rather than densely (Fig. 6a, b, f), reflecting that the macropores developed overall poorly in the coal samples. Besides, it was found that some macropores were filled with clay minerals that were not completely dissolved (Fig. 6e, f). The distribution of mesopores was relatively dispersed (Fig. 6a, b, d) or dense (Fig. 6c). The areal density of mesopores was higher than the macropores, indicating that the mesopores were better developed than the macropores. Compared with macropores and mesopores, the micropores and transition pores (MIT) were widely and densely distributed in the coal samples (Fig. 6d, h–j). We used the software Avizo to visualize the pores in a FE-SEM image (Fig. 6h'–j'). Meanwhile, the sizes of the pores were measured and counted through this software. From three FE-SEM images of coal samples, it was found that pores with diameters between 10–20 nm were well-developed (Fig. 6h''–j'').

The fractures in coals can be endogenous or exogenous in origin (Zhang et al. 2018). The dehydration and devolatilization processes of gelation materials during the process of coalification cause the coal matrix to shrink, which brings about the generation of endogenous fractures (also known as cleats) (Chen et al. 2015), whereas the formation of exogenous fractures is related to tectonic stress. The Eastern Surat Basin coals exhibited well-developed endogenous fractures (Fig. 7a–f) under the FE-SEM. Some coal samples contained two groups of main endogenous fractures, and they were nearly perpendicular (Fig. 7a–d); each group was arranged in parallel. The endogenous fractures usually broke down when the coal composition changed (Fig. 7a, e). Exogenous fractures also existed in the coal

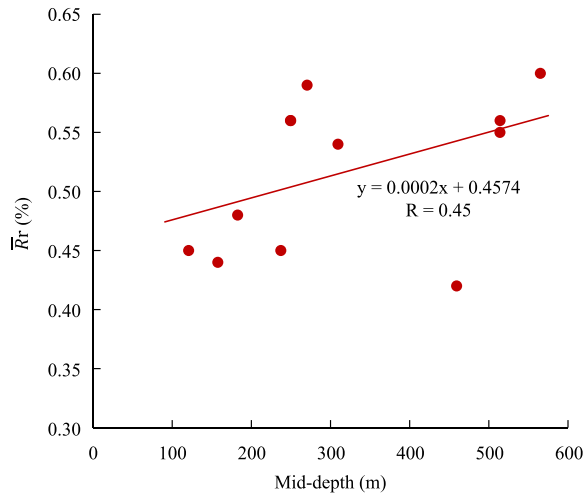


**Figure 4.** Relationship between the  $\bar{R}_r$  and mid-depth of sampled Surat coals.

samples (Fig. 7g–i), and they were tensile (Fig. 7g, h) or shear fractures (Fig. 7i). Some tensile fractures were arranged in echelon and intersected with the main fracture (Fig. 7g). The shear fractures had smoother faces (Fig. 7i). It was found that the fractures in the coal samples were usually filled with minerals to varying degrees (Fig. 7d, h, i). The energy spectrum analysis show that the minerals were clay minerals (kaolinite or illite). Using the software Avizo, it was found that whether it is endogenous or exogenous fracture, the widths of fractures in the coal samples were generally greater than 1  $\mu\text{m}$  (Fig. 7).

### Pore–Fracture Size Distribution Identified By NMR

Figure 8 shows the NMR  $T_2$  spectrums of all the coal samples from the Eastern Surat Basin under the  $S_f$  and  $S_{ir}$  conditions. The  $T_2$  values of coal samples under the  $S_f$  condition ranged from 0.01 to 10000 ms approximately. Except for the sample Su-10 (double peaks,  $p_1$  and  $p_2$ ), the other samples under the  $S_f$  condition all had three peaks ( $p_1$ ,  $p_2$  and  $p_3$ )  $T_2$  spectrums, and the amplitude of  $p_1$  was significantly higher than that of  $p_2$  and  $p_3$ . Only two samples (Su-3 and Su-4) had double peaks  $T_2$  spectrum under the  $S_{ir}$  condition, while most coal samples had an unimodal ( $p_1$ )  $T_2$  spectrum. The cumulative amplitudes of  $T_2$  spectrums for all the samples under the  $S_f$  condition were significantly greater than those under the  $S_{ir}$  condition.

In a  $T_2$  spectrum of a coal under the  $S_f$  condition, there is a boundary  $T_2$  value, named  $T_{2C}$ , that divides the  $T_2$  spectrum into movable water and restrained water parts (Yao et al. 2010a). The movable water has the value of  $T_2 > T_{2C}$  and corresponds to seepage pores, in which the water can be basically drained, while the restrained water possesses the value of  $T_2 < T_{2C}$  and corresponds to adsorption pores, where the water cannot be drained easily because of capillary forces. The accurate measurement of  $T_{2C}$  is a key step in estimating the movable water and restrained water volume proportions, as well as the pore–fracture size distribution.

The procedure for determining the  $T_{2C}$  value is shown in Figure 9 using the coal sample Su-11 as an example. First, the cumulative porosity curves of NMR  $T_2$  spectrums under the  $S_f$  and  $S_{ir}$  conditions were drawn, respectively; next, a line parallel to the X-axis was drawn from the maximum value of the cumulative porosity curve of  $S_{ir}$ , and this line intersected with the cumulative porosity curve of  $S_f$ ; finally, a line perpendicular to the X-axis was drawn from the intersection point, and the corresponding X value was  $T_{2C}$  (Fig. 9). By using this method, the  $T_{2C}$  value of the coal sample Su-11 was determined as 0.901 ms. Thus, Table 3 displays the  $T_{2C}$  values for the additional coal samples. The results show that the  $T_{2C}$  values of the Eastern Surat Basin coals ranged from 0.314 to 1.060 ms, with average of 0.690 ms.

By using the  $T_{2C}$ , the pore–fracture size distribution of coal can be determined, and the basic principle is that: for all the coal samples, the pore diameter corresponding to the  $T_{2C}$  is definite (Yao et al. 2010b). If the pore diameter of coal corresponding to the  $T_{2C}$  is a constant  $d$ , then the pore diameter  $d_{ci}$  corresponding to the  $i$ th relaxation time  $T_{2i}$  can be expressed as (Yao et al. 2010b):

$$d_{ci} = dT_{2i}/T_{2C} \quad (4)$$

In addition, according to Washburn's equation:

$$r_c = -2\sigma \cos \theta / P_c \quad (5)$$

where  $r_c$  represents the minimum pore radius corresponding to the drainage water under centrifugal pressure  $P_c$ ;  $\theta$  is the contact angle between the water and the pore surface of coal;  $\sigma$  is the surface tension between coal and water. Based on previous studies (Fu et al. 1997),  $\theta$  and  $\sigma$  were assigned as  $60^\circ$  and 0.076 N/m. Hence, Eq. 5 can be simplified as:



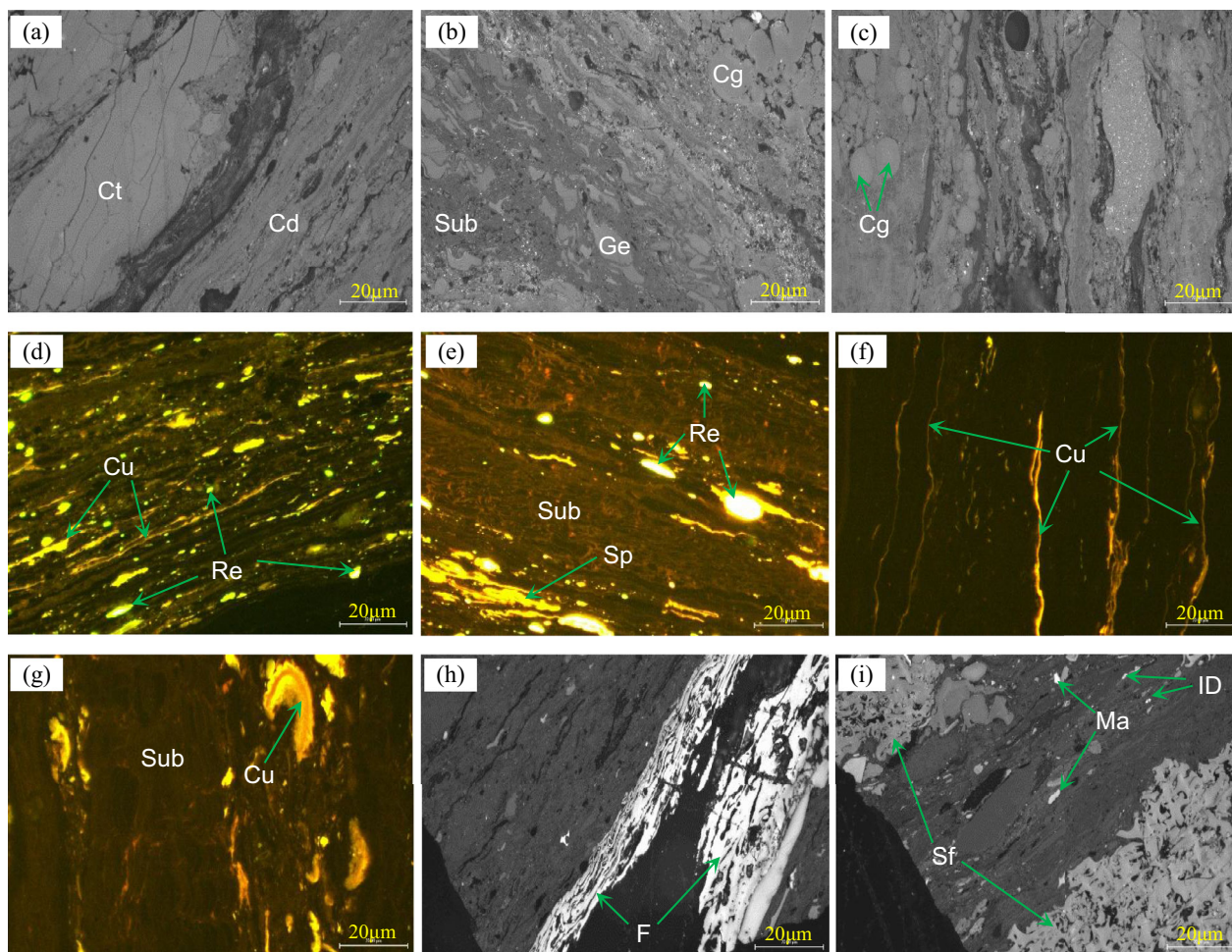


**Figure 5.** Macerals in some coal samples from Eastern Surat Basin. (a) Su-2; (b) Su-4; (c) Su-4; (d) Su-7; (e) Su-6; (f) Su-10; (g) Su-10; (h) Su-9; (i) Su-9. *Ct* collotelinite, *Cg* corpogelinite, *Cd* collodetrinite, *Ge* gelocollinite, *F* fusinite, *Sf* semifusinite, *Ma* macrinite, *ID* inertodetrinite, *Sp* sporinite, *Cu* cutinite, *Re* resinite, *Sub* suberinite.

$$r_c = 0.14/P_c \tag{6}$$

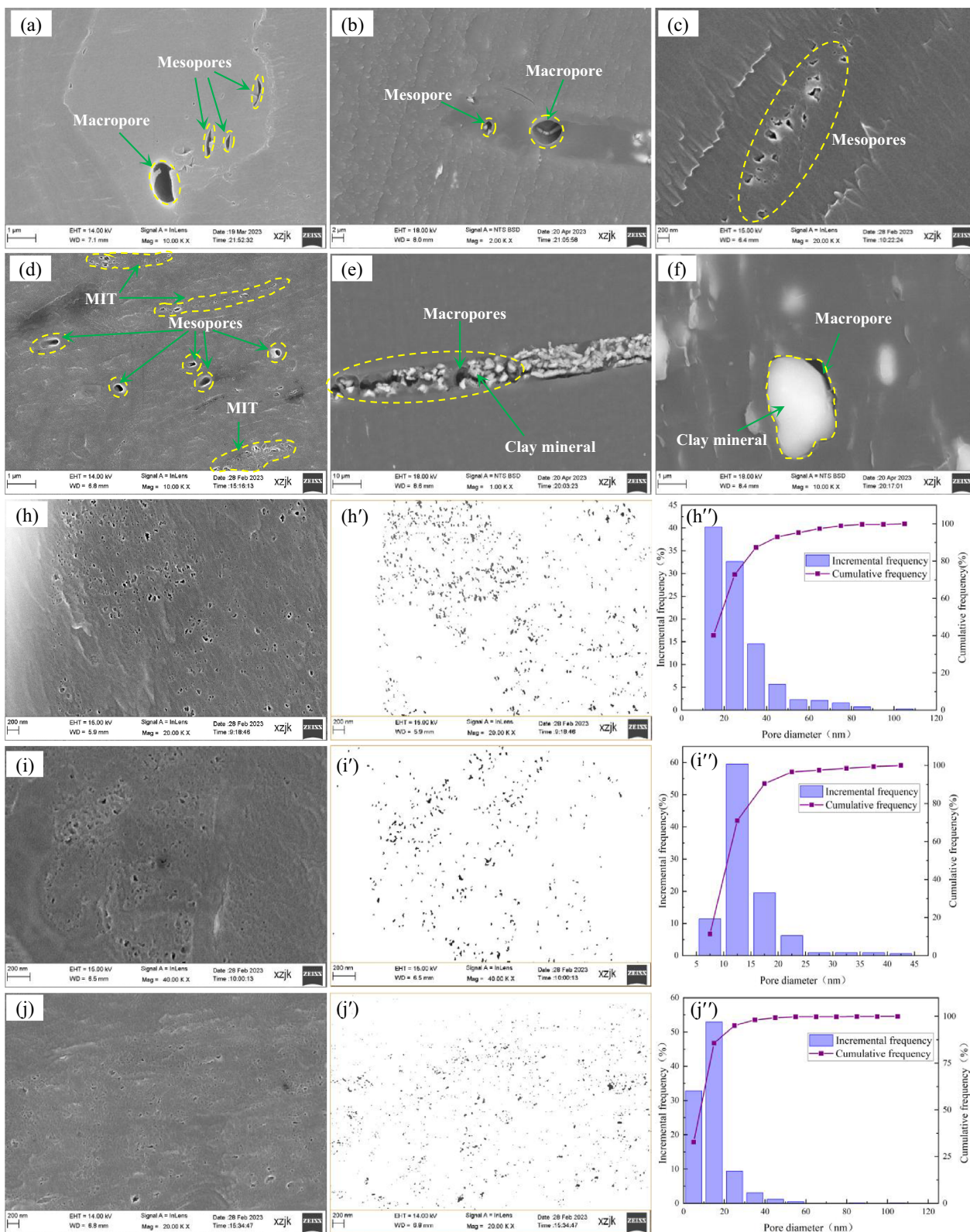
Equation 6 demonstrates that the  $r_c$  is directly relevant to the centrifugal pressure. As stated in “NMR Experiments” section, the centrifugal pressure used in this work was 2.65 MPa, corresponding to a pore radius of 53 nm (diameter = 106 nm) through the calculation of Eq. 6. This indicates that the pore diameter  $d$  of coal corresponding to the  $T_{2C}$  in Eq. 4 was 106 nm. In addition, the  $T_{2C}$  value of each sample is listed in Table 3. Thus, Eq. 4 can be used to determine the  $d_{ci}$  values of various relaxation times  $T_{2i}$  for a particular coal sample. Consequently, the pore–fracture size distribution of a specific coal sample can be determined through the NMR  $T_2$  spectrum under the  $S_f$  condition.

Figure 10 displays all 12 coals’ calculated pore–fracture size distribution curves and the volume

proportions of each pore–fracture structure type. It was found that the pore–fracture structure of Eastern Surat Basin coals was characterized by an overwhelming predominance of MIT (micropore and transition pore) in the total pore–fracture volume, and less developed and approximate volume proportion of mesopore (ME) and MAF (macropore and fracture). The volume proportions of MIT, ME and MAF were 51.38–94.07% (avg. 74.58%), 3.88–31.36% (avg. 14.06%) and 1.84–18.81% (avg. 11.36%), respectively.

### Porosity and Movable Porosity Analyzed By NMR

The CSG is produced through the pore–fracture system of coal at all levels; therefore, its structural



◀ **Figure 6.** FE-SEM images of pores in some coal samples from Eastern Surat Basin coals: (a–d), images showing some macropores and mesopores; (e, f), macropores filled with clay minerals; (h–j), images showing micropores and transition pores (MIT); (h'–j'), the pores distribution of images (h–j) processed by Avizo software; (h''–j''), the diameter statistics of pores in the images (h'–j').

characteristics and development scale of pore–fracture play decisive roles in determining the coal permeability. Porosity, which includes both connected and partially closed pore–fractures in coal is generally used as an indicator of the overall development scale of pore–fractures (Yao et al. 2010a). In this study, NMR experiments were used to measure the porosities of coals from the Eastern Surat Basin. As stated in “NMR experiments” section, the water volume  $V_w$  in the fully saturated water sample can be determined using the CA of the NMR  $T_2$  spec-

trum under the  $S_f$  condition, and then the porosity  $\phi_t$  of coal can be obtained as:

$$\phi_t = \frac{V_w}{V_s} = \frac{M_f}{22765 \times V_s} \quad (7)$$

where  $\phi_t$  is coal porosity (%),  $V_w$  is water volume (mL) in the fully saturated water sample,  $V_s$  is volume ( $\text{cm}^3$ ) of the fully saturated water sample, and  $M_f$  is the CA of NMR  $T_2$  spectrum under the  $S_f$  condition. Hence, the porosity of each pore–fracture structure type of coal can be calculated as:

$$\phi_{ti} = \phi_t \times V_i = \phi_t \times \frac{\sum M_{fi}}{M_f} \quad (8)$$

where  $V_i$  represents the volume proportion (%) of a particular pore–fracture structure type, and  $i$  can be MIT, ME or MAF;  $\phi_{ti}$  is porosity (%) of a particular pore–fracture structure type,  $\sum M_{fi}$  is the CA of

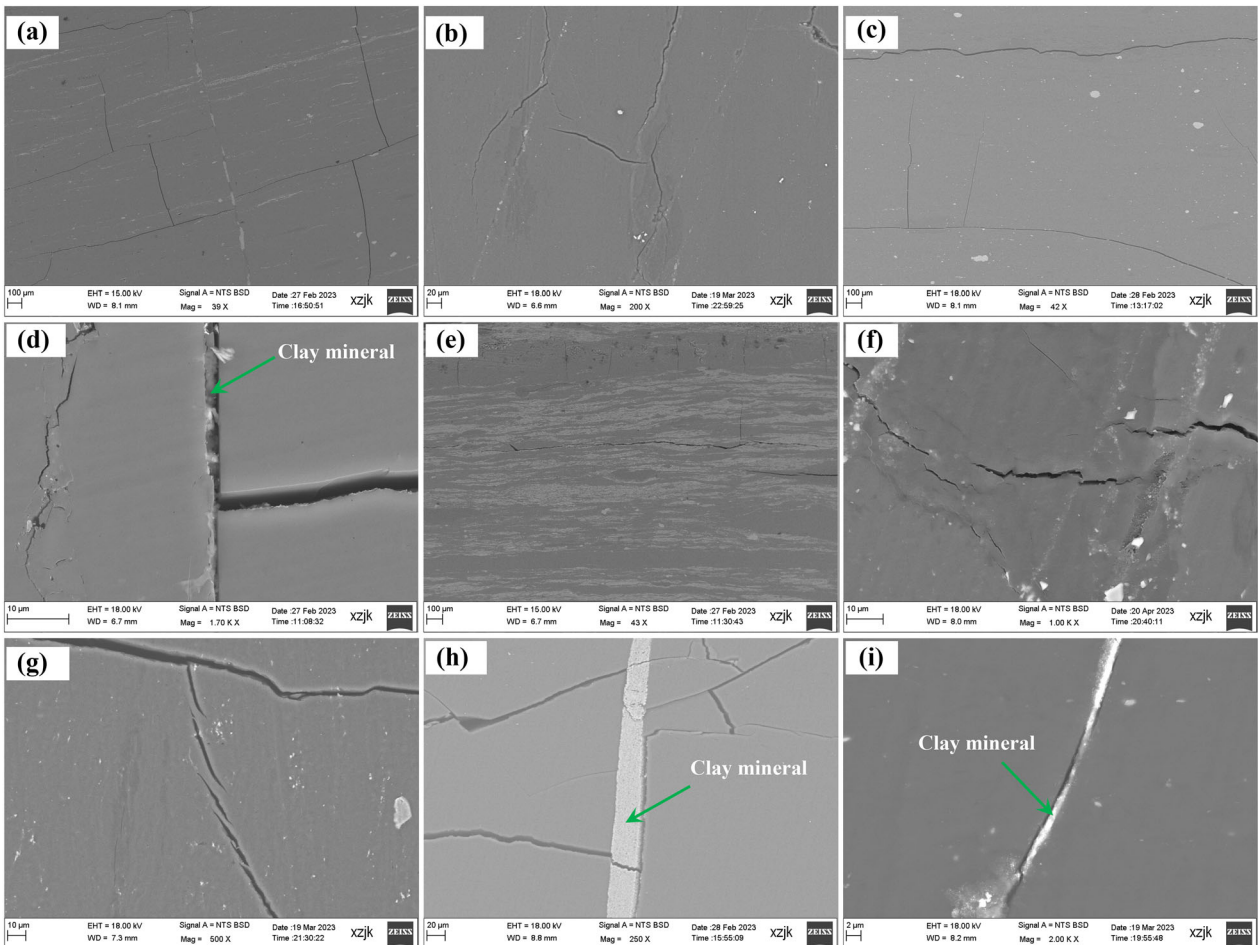


**Figure 7.** FE-SEM images of fractures in some coal samples from Eastern Surat Basin coals.

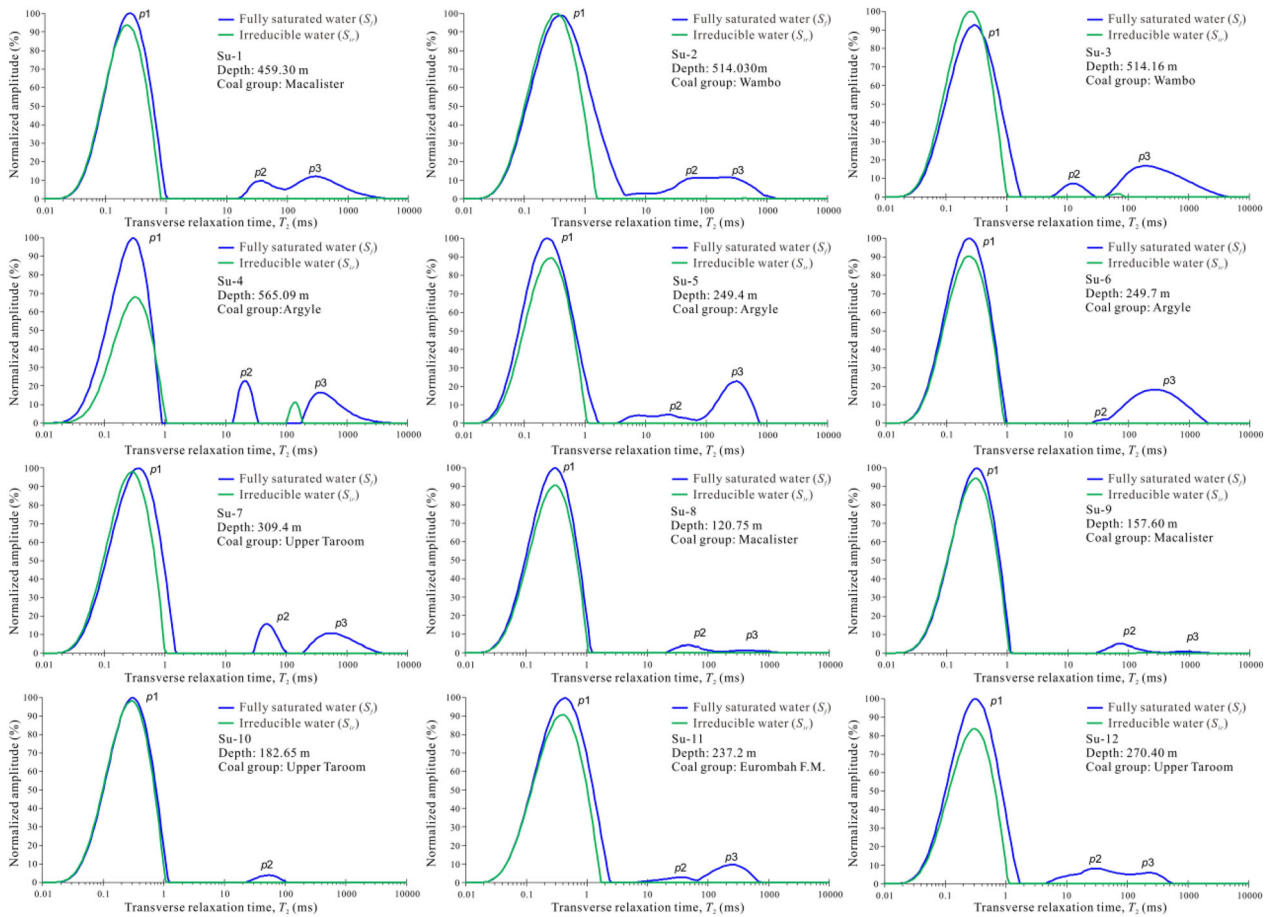


Figure 8. NMR  $T_2$  spectra of the sampled Eastern Surat Basin coals under the  $S_f$  and  $S_{ir}$  conditions.

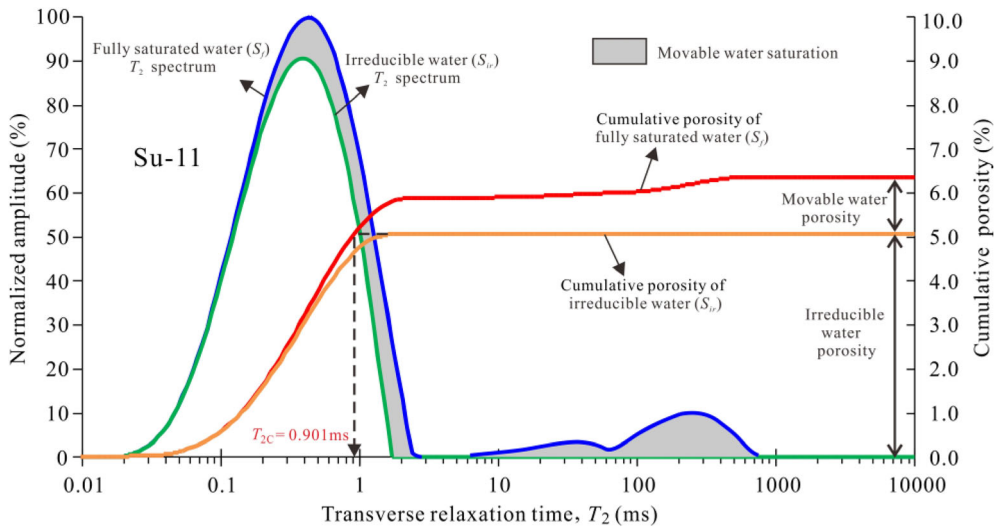


Figure 9. Method of obtaining  $T_{2C}$  value of coal sample in the NMR experiment (sample Su-11).

**Table 3.** Related parameters of the sampled Eastern Surat Basin coals obtained from NMR experiments

Sample I.D.	$T_{2C}$ (ms)	Volume proportion in total pore–fracture (%)			$\varphi_t$ (%)	$\varphi_m$ (%)	$\varphi_t$ (%)			$\varphi_m$ (%)			$S_{mw}$ (%)
		MIT	ME	MAF			MIT	ME	MF	MIT	ME	MAF	
Su-1	0.533	73.15	11.32	15.53	4.40	1.03	3.22	0.50	0.68	0.15	0.21	0.67	23.41
Su-2	1.060	71.50	16.05	12.45	5.41	1.42	3.87	0.87	0.67	0.05	0.70	0.67	26.25
Su-3	1.060	77.31	3.88	18.81	3.99	0.86	3.08	0.15	0.76	0	0.15	0.71	21.55
Su-4	0.314	51.38	31.36	17.26	1.10	0.46	0.57	0.34	0.19	0.23	0.06	0.17	41.82
Su-5	0.511	68.37	16.05	15.58	3.44	1.03	2.35	0.55	0.54	0.34	0.16	0.54	29.94
Su-6	0.511	72.04	9.60	18.36	3.17	0.85	2.28	0.30	0.59	0.20	0.06	0.59	26.81
Su-7	0.737	74.55	13.25	12.20	2.93	0.63	2.18	0.39	0.36	0.01	0.26	0.36	21.50
Su-8	0.578	80.49	16.16	3.35	6.94	1.02	5.59	1.12	0.23	0.55	0.24	0.23	14.70
Su-9	0.737	88.64	8.07	3.29	7.53	0.61	6.67	0.61	0.25	0.22	0.14	0.25	8.10
Su-10	0.831	94.07	4.09	1.84	7.38	0.34	6.95	0.3	0.13	0.09	0.12	0.13	4.61
Su-11	0.901	76.84	15.74	7.42	6.37	1.31	4.89	1.01	0.47	0.38	0.46	0.47	20.57
Su-12	0.511	66.56	23.20	10.24	8.30	2.52	5.53	1.92	0.85	0.84	0.83	0.85	30.36

MIT (< 100 nm) = micropore and transition pore; ME (100–1000 nm) = mesopore; MAF (> 1000 nm) = macropore and fracture;  $\varphi_t$  = porosity (%);  $\varphi_m$  = movable porosity (%);  $S_{mw}$  = movable water saturation (%).

NMR  $T_2$  spectrum of a particular pore–fracture structure type under the  $S_f$  condition.

The porosity of coal includes movable porosity and irreducible porosity (Yao et al. 2010a). The coal’s movable porosity can be calculated through the CAs of the NMR  $T_2$  spectrums under the  $S_f$  and  $S_{ir}$  conditions (Fig. 8). The calculation equation is:

$$\varphi_m = \varphi_t \frac{M_f - M_r}{M_f} \tag{9}$$

where  $\varphi_m$  is the coal’s movable porosity (%) and  $M_r$  is the CA of the NMR  $T_2$  spectrum under the  $S_{ir}$  condition. Hence, the movable porosity of each pore–fracture structure type of coal can be determined as:

$$\varphi_{mi} = \frac{\sum M_{fi} - \sum M_{ri}}{\sum M_{fi}} \times \varphi_{ti} \tag{10}$$

where  $\varphi_{mi}$  is the movable porosity (%) of a particular pore–fracture structure type, and  $\sum M_{ri}$  is the CA of NMR  $T_2$  spectrum of a particular pore–fracture structure type under the  $S_{ir}$  condition. The coal’s movable water saturation can be determined as:

$$S_{mw} = \frac{M_f - M_r}{M_f} \tag{11}$$

According to Eqs. 7 to 11, the porosities, movable porosities and movable water saturations for the Eastern Surat Basin coals are calculated and shown in Table 3, as well as the porosities and

movable porosities of different pore–fracture structure types. The results showed that the coals’ porosities ranged 1.10–8.30%, with average of 5.08%. The movable porosities ranged 0.34–2.52%, averaging 1.01%. The movable water saturations ranged 4.61–41.82%, averaging 22.47%. The results of the correlation analysis showed a positive correlation between the samples’ movable porosities and porosities; however, the correlation was poor with  $R^2$  of only 0.20, indicating that the coal with higher porosity does not necessarily possess a higher movable porosity, which is related to the coal’s pore–fracture structure.

The results of porosities and movable porosities of different pore–fracture structure types (Table 3, Fig. 11) showed that the porosity ranges of MIT, ME and MAF were 0.57–6.95% (avg. 3.93%), 0.50–1.92% (0.67%) and 0.13–0.85% (avg. 0.48%), respectively. The movable porosity ranges of MIT, ME and MAF were 0–0.84% (avg. 0.26), 0.06–0.83% (avg. 0.28%) and 0.13–0.85% (avg. 0.47%), respectively. Therefore, it was found that the porosity of MIT was absolutely dominant among the three types of pore–fracture structure; however, only an average of 6.6% of space in the MIT was movable. In contrast, although the porosity of MAF was the lowest, almost all the space (an average of 97.9%) in the MAF was movable, and its movable porosity was the highest as a whole. For the ME, both its porosity and movable porosity were between MIT and MAF, and average of 41.8% of space in the ME was movable. Figure 12 shows that the movable porosities of

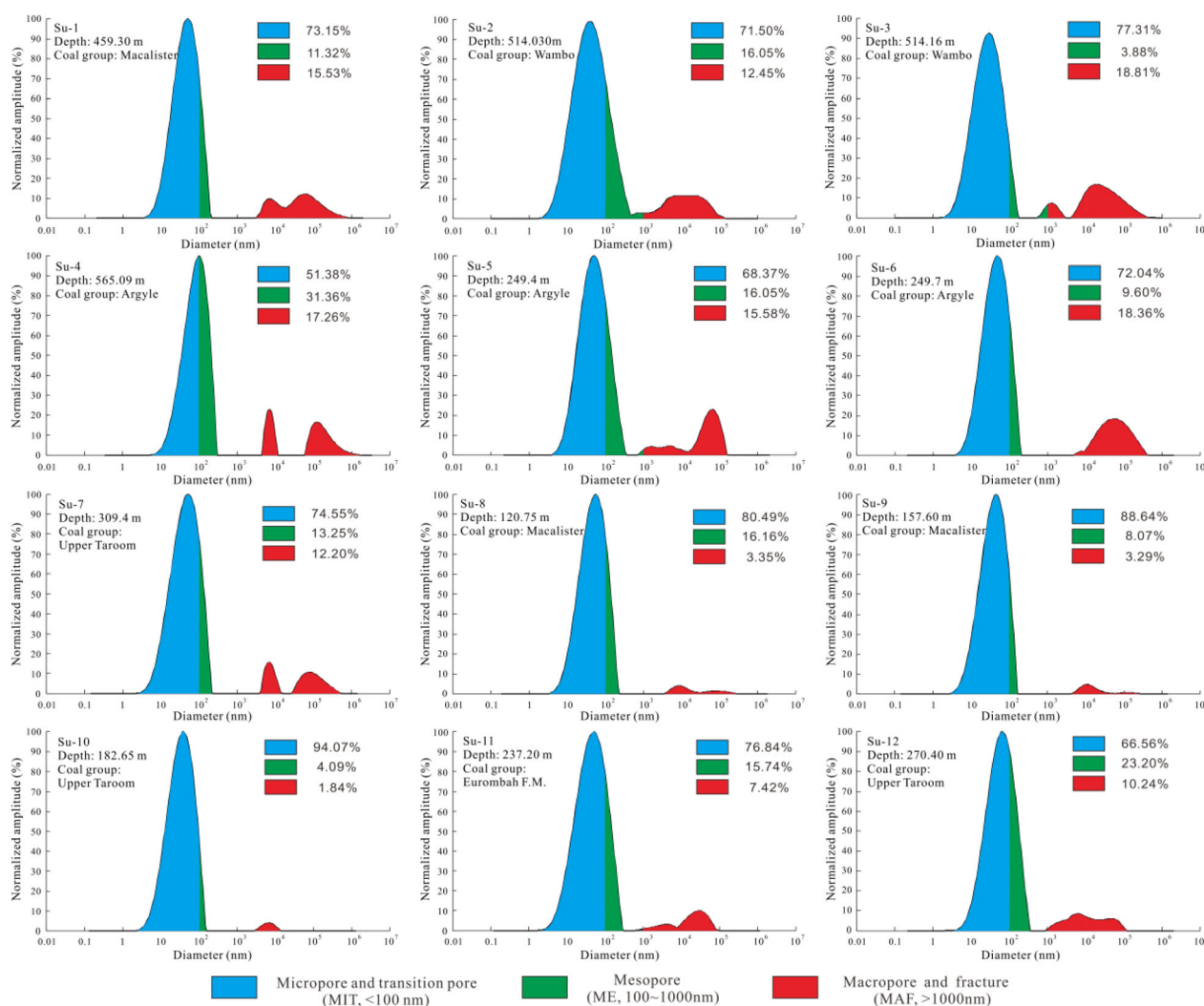


**Figure 10.** Pore diameter distributions of the sampled Eastern Surat Basin coals obtained from NMR experiments and the volume proportion of each pore–fracture structure.

Eastern Surat Basin coals exhibited excellent positive correlation with the sum of the porosities of ME and MAF, indicating that the more developed the MAF and ME, the higher the movable porosity and the possibly higher the coal permeability (Zhang et al. 2018).

## DISCUSSIONS

### Effect of Coal Maturity on Pore–Fracture Structure

The coal maturity has an impact on the pore–fracture structure development characteristics of

coals (Li et al. 2017a; Tao et al. 2018). Generally, coal maturity increases with vitrinite reflectance (Zielar et al. 2018; Zhang et al. 2023). Based on the correlativity (Fig. 13) between the  $\bar{R}_r$  and the pore–fracture structure of Eastern Surat Basin coals, it can be inferred that the volume proportion of MIT was relatively low in the lignite stage ( $\bar{R}_r < 0.4\%$ ), and in contrast, plenty of ME (mesopores) and macropores existed. This is because the pores' physical compaction degree was weaker due to the relatively low overlying formation pressure. Meanwhile, because of the low degree of gelatination in the lignite stage, the endogenous fractures (i.e., cleats) created by coal matrix shrinkage were less common; thus,

the MAF in the lignite stage was mainly composed of macropore under the condition without tectonic transformation. The volume proportions of ME and macropores decreased gradually (Fig. 13b, c) when thermal evolution increased in the stage of subbituminous coal ( $0.40\% \leq \bar{R}r < 0.50\%$ ) for two reasons. One is physical compaction caused by the increase in overlying formation pressure (Xin et al. 2022), and the other is chemical cementation (Fu et al. 2016). In contrast, the volume proportion of MIT increased gradually (Fig. 13a). When the  $\bar{R}r$  reached about 0.5%, the volume proportion of seepage pores (including ME and MAF,  $> 100\text{ nm}$ ) decreased to the lowest level, whereas the volume proportion of MIT increased to the highest level. The dehydration, devolatilization and coal matrix shrinkage processes got stronger as coalification progressed, resulting in a significant increase of endogenous fractures in coals, and the fracture density increases in the stage of bituminous coal D ( $0.50\% \leq \bar{R}r < 0.60\%$ ) (Su et al. 2001). This study demonstrated that the volume proportion of MAF increased as  $\bar{R}r$  rose from 0.50 to 0.60% (Fig. 13c) because of the increase in endogenous fractures. Meanwhile, the volume proportion of ME also increased (Fig. 13b) when  $\bar{R}r$  rose from 0.50 to 0.65% possibly because of the further compaction of macropore and the change into ME. The volume proportion of MIT decreased as a result of the volume proportion increases in ME and MAF (Fig. 13a).

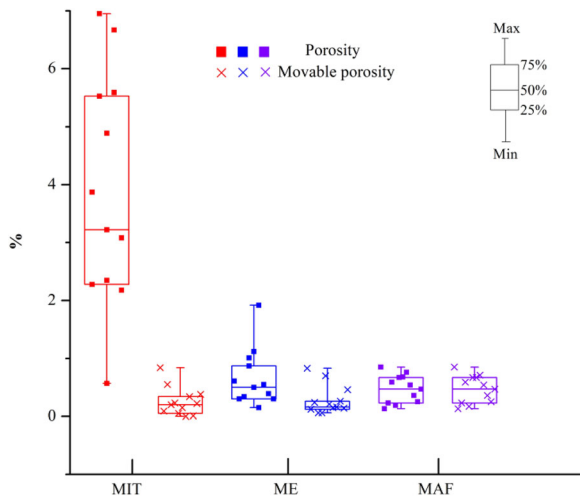


**Figure 11.** Porosity and movable porosity distributions of different pore–fracture structure types for the sampled Eastern Surat Basin coals.

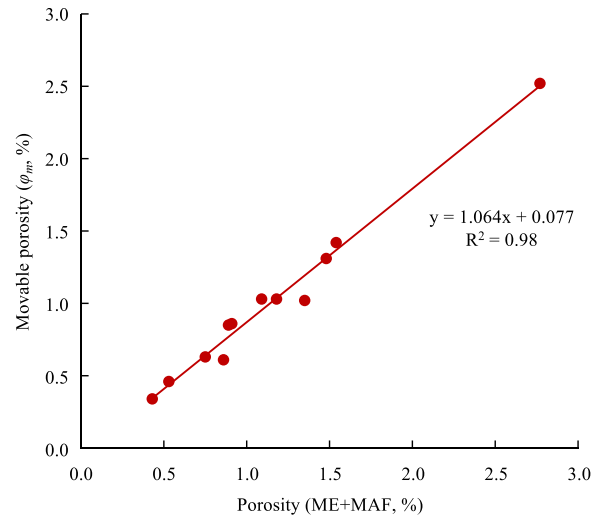


**Figure 12.** Relationship between the movable porosity and the sum of ME and MAF porosity for the sampled Eastern Surat Basin coals.

### Effect of Coal Macerals on Pore–Fracture Structure

It was known, based on the results of FE-SEM experiments, that some fractures in Eastern Surat Basin coals were filled with clay minerals to varying degrees, and at the same time, residual minerals that were not completely dissolved were found in some macropores. The presence of minerals will unavoidably occupy some of fractures and macropores spaces in the coals of the study area, reducing their volume proportion in the total pore–fracture spaces. Figure 14a shows that the volume proportion of MAF presents a decreasing trend with increase in mineral contents in the sampled coals when eliminating the abnormal point of sample Su-9.

Differences exist in the pore–fracture structure characteristics among the different organic macerals in coals (Shen et al. 2019; Han et al. 2021). The volume proportion of MAF, except the abnormal point of sample Su-10 (Fig. 14b), showed an increasing trend with rise in vitrinite content, suggesting that the coals with higher vitrinite contents had a higher volume proportion of MAF (Fig. 14b). Previous researches generally believed that fractures in coals are the result of the combined effect of internal and external forces (Laubach et al. 1998; Qu et al. 2022). Compared with other organic macerals, the vitrinite has greater brittleness and is more likely to generate exogenous fractures when subjected to external forces (Su et al. 2001). Besides, during the process of coalification, vitrinite easily generates

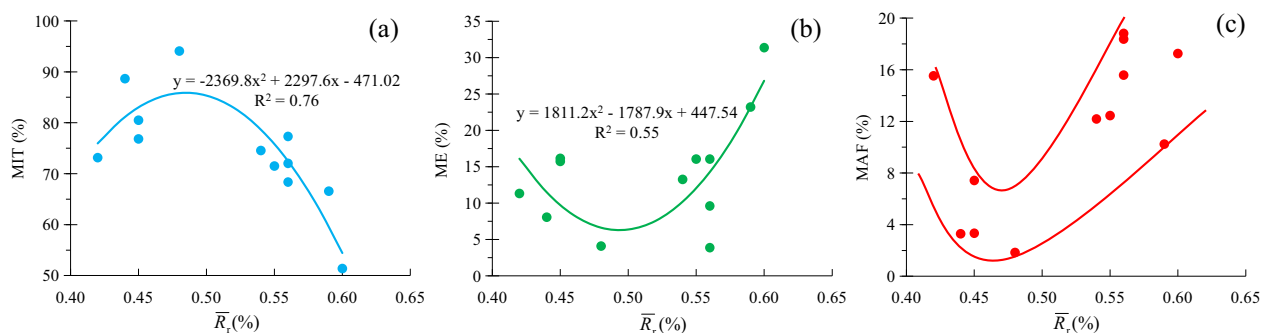


**Figure 13.** Relationships between  $\bar{R}_r$  and volume proportion of each pore–fracture structure (a MIT; b ME; c MAF) of sampled Eastern Surat coals.

endogenous fractures (also known as cleats) with dehydration, devolatilization and coal matrix shrinkage processes (Liu et al. 2021). Therefore, fractures are well-developed in the vitrinite.

### Effect of Coal-Forming Environments on Coal Porosity

Different coal-forming environments have diverse vegetation combination types, hydrogeological conditions and sediment provenances, etc., which may affect coals' pore–fracture structure characteristics (Zhang et al. 2010). The coal-forming environment can be characterized by coal facies parameters, commonly including texture preservation index (TPI), gelation index (GI), groundwater flow index (GWI) and vegetation index (VI) (Diesel 1982; Calder et al. 1991). These parameters can well reflect some information during peat accumulation, such as coal-forming plants, swamp medium conditions, depositional environments, etc. (Zhao

et al. 2016a, 2016b; Jiu et al. 2021). The coal facies parameters TPI, GI, GWI and VI can be calculated through the following equations (Dai et al. 2007):

The TPI can reflect the degree of preservation or destruction of plant tissue structure (Zhao et al. 2016a, 2016b). In general, greater TPI values indicate better preservation of plant tissue structure, which suggests weaker physical crushing and chemical degradation of plant remains in the swamp. The relationship between TPI and porosities of Eastern Surat Basin coals (Fig. 15a) shows that the porosity overall increases with rise in TPI, indicating that coals with better plant tissue structure generally have higher porosities.

GI mainly indicates the dampness degree of peat swamp. In general, greater GI indicates higher gelatination degree and deeper water that covers the swamp. Because the inertinite compositions are generally rare in the sampled Eastern Surat Basin coals, only a small amount of inertinite compositions such as fusinite and semifusinite were detected in

$$GI = \frac{\text{vitrinite} + \text{macrinite}}{\text{semifusinite} + \text{fusinite} + \text{inertodetrinite}}$$

$$TPI = \frac{\text{telinite} + \text{collotelinite} + \text{fusinite} + \text{semifusinite}}{\text{collodetrinite} + \text{macrinite} + \text{inertodetrinite} + \text{vitrodetrinite} + \text{corpogelinite}}$$

$$GWI = \frac{\text{gelocollinite} + \text{corpogelinite} + \text{mineral} + \text{vitrodetrinite}}{\text{telinite} + \text{collotelinite} + \text{collodetrinite}}$$

$$VI = \frac{\text{telinite} + \text{collotelinite} + \text{fusinite} + \text{semifusinite} + \text{funginite} + \text{secretinite} + \text{resinite}}{\text{collodetrinite} + \text{inertodetrinite} + \text{alginate} + \text{liptodetrinite} + \text{cutinite}}$$



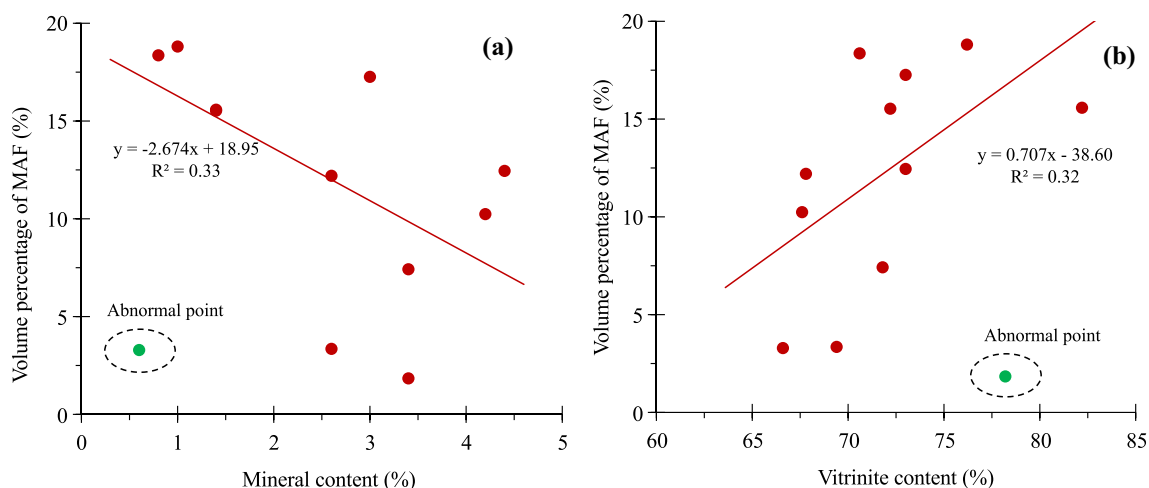


**Figure 14.** Scatter plots between volume percentages of MAF and mineral (a), and vitrinite contents (b) for the sampled Eastern Surat Basin coals.

five coal samples, and the remaining samples have no inertinite compositions detected. Therefore, the GI values of only these five samples were calculated in this study. The volume proportion of MIT was observed to decrease as the GI increased (Fig. 16a), while the MAF shows a diametrically opposite change (Fig. 16b). This is because higher GI means higher gelatination degree and more vitrinite contents, and “Effect of coal-forming environments on coal porosity” section discussed that Eastern Surat Basin coals with higher vitrinite contents have more MAF. In addition, the GI presented a good negative correlation with the porosities of coals (Fig. 15b), reflecting that the deeper water that covers the swamp, the possibly lower the porosities of coals that were formed.

GWI reflects the groundwater level during the peat accumulation and the degree of groundwater control over the peat swamp. In general, a higher GWI indicates a higher groundwater level, which means more groundwater supply for the peat swamp and thus more mineral accumulation during the coal-forming period. As discussed in “Effect of coal-forming environments on coal porosity” section, the minerals in coals occupy some of the pore–fracture spaces of coals, leading to the decreases of porosities. The GWI of sampled Eastern Surat Basin coals were generally low with values varying from 0.116 to 0.407, suggesting that the groundwater level was overall low during the peat accumulation and the groundwater recharge to the peat swamp was weak on the whole, which leads to a weak negative cor-

relation between the GWI and the porosities of the coal samples in this study (Fig. 16c).

The VI is associated with the type of coal-forming plants, and it shows the ratio of macerals with forest woody affinity to herbaceous or aquatic affinity (Thompson et al. 1985). In general, a higher VI denotes the presence of more woody forest plants and fewer herbaceous or aquatic plants in the coal-forming plants. The VI of sampled Eastern Surat Basin coals overall showed a positive correlation with porosities (Fig. 16d), suggesting coals formed with more forest woody plants have higher porosities. The forest woody plants have plenty of lignin than herbaceous or aquatic plants, which results in a higher degree of lignification and harder texture, which are more conducive to the preservation of plant tissue structure. As a result, coals formed with more forest woody plants may have higher porosities.

## CONCLUSIONS

In this study, to evaluate the pore–fracture structure characteristics of 12 coals from Eastern Surat Basin, coal petrology analysis, FE-SEM and NMR experiments were carried out. The conclusions are as follows:

1. The sampled coals belong to low-medium rank coals, with  $\bar{R}_r$  ranging 0.42–0.60%. The porosities of the coals ranged 1.10–8.30% (avg. 5.08%).

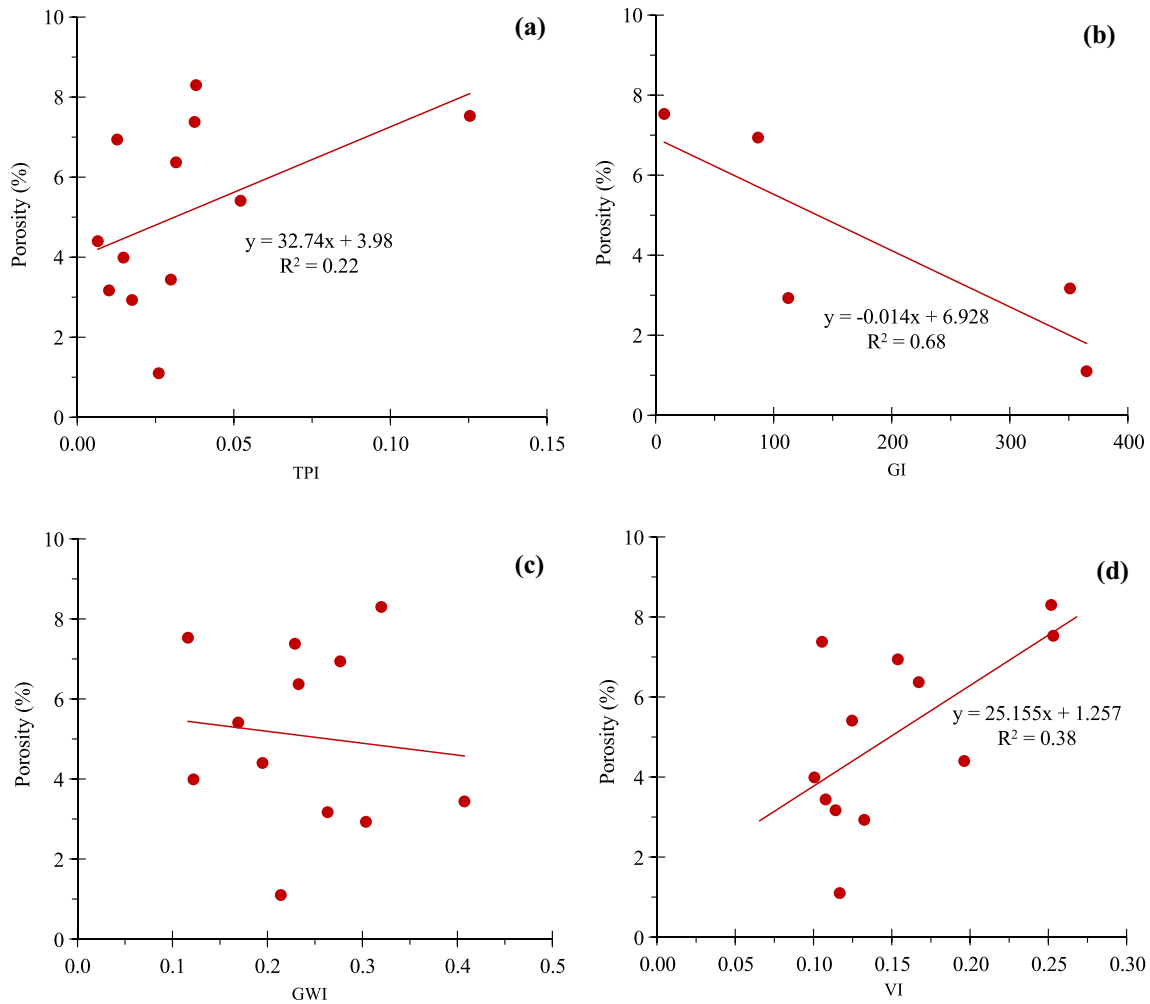


**Figure 15.** Scatter plots between coal facies parameters (a) TPI; b) GI; c) GWI; d) VI and porosities of the sampled Eastern Surat Basin coals.

- The pore–fracture structure of the coals is characterized by an overwhelming predominance of MIT, and less developed and approximate volume proportion of ME and MAF, with average volume proportions of 74.58%, 14.06%, and 11.36%, respectively.
- The movable porosities of the coals ranged 0.34–2.52% (avg. 1.01%). Meanwhile, the movable porosities of different pore–fracture structure types were calculated, and the average values are presented as MAF > ME > MIT. The average movable spaces in the MIT, ME and MAF of the coals were 6.6%, 41.8% and 97.9%, respectively.
  - As coal maturity increases, the volume proportions of MIT show an inverted U-shape change of first increase and then decrease, while the volume proportions of both ME and MAF take on an opposite change, presented as U-shape, and the turning points all occur at  $\bar{R}r$  of approximately 0.5%.
  - The volume proportion of MAF is higher in coals with higher vitrinite and lower mineral contents. The coal facies have some impacts on the porosities of the Surat Basin coals, and the coals with higher TPI and VI, and lower GI values overall have higher porosities.

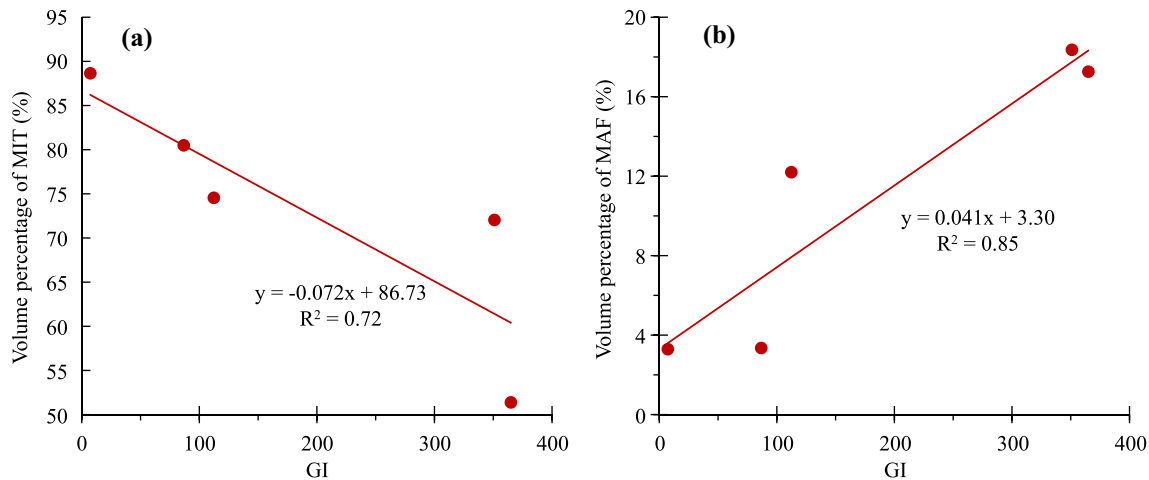


Figure 16. Relationship between GI and volume percentage of MIT (a) and MAF (b).

## ACKNOWLEDGMENTS

This work was financially supported by the commissioned project of PetroChina Research Institute of Petroleum Exploration & Development (No. RIPED-2022-JS-1301), and the National Natural Science Foundation of China (No. 42130802).

## DECLARATIONS

**Conflict of Interest** The authors declare that there is no conflict of interest regarding the publication of this paper.

## REFERENCES

- Andrade, C., Sobczak, K., Vasconcelos, P., Holl, H. G., Hurter, S., & Allen, C. M. (2023). U-Pb detrital zircon geochronology of the Middle to Upper Jurassic strata in the Surat Basin: New insights into provenance, paleogeography, and source-sink processes in eastern Australia. *Marine and Petroleum Geology*, *149*, 106122.
- Ayers Jr, W. B. (2002). Coalbed gas systems, resources, and production and a review of contrasting cases from the San Juan and Powder River basins. *AAPG Bulletin*, *86*, 1853–1890.
- Calder, J. H., Gibling, M. R., & Mukhopadhyay, P. K. (1991). Peat formation in a Westphalian B piedmont setting, Cumberland Basin, Nova Scotia: Implications for the maceral-based interpretation of rethrophic and raised paleomires. *Bulletin de la Société Géologique de France*, *162*(2), 283–298.
- Chen, Y., Tang, D. Z., Xu, H., Tao, S., Li, S., Yang, G. H., & Yu, J. J. (2015). Pore and fracture characteristics of different rank coals in the eastern margin of the Ordos Basin, China. *Journal of Natural Gas Science and Engineering*, *26*, 1264–1277.
- Cheng, Y. P., & Hu, B. (2023). A new pore classification method based on the methane occurrence and migration characteristics in coal. *Journal of China Coal Society*, *48*(1), 212–225. in Chinese.
- Coates, G. R., Xiao, L. Z., & Prammer, M. G. (1999). *NMR logging principles and applications*. Gulf Publishing Company.
- Cui, Z. H., Su, P. H., Liu, L. L., Li, M., & Wang, J. J. (2022). Quantitative characterization, exploration zone classification and favorable area selection of low-rank coal seam gas in Surat block in Surat Basin, Australia. *China Petroleum Exploration*, *27*, 108–118. in Chinese.
- Dai, S. F., Ren, D. Y., Li, S. S., Zhao, L., & Zhang, Y. (2007). Coal facies evolution of the main minable coal-bed in the Heidaigou Mine, Jungar Coalfield, Inner Mongolia, northern China. *Science in China Series D-Earth Sciences*, *50*, 144–152.
- Diessel, C. F. K. (1982). An appraisal of coal facies based on maceral characteristics. *Australian Coal Geology*, *4*(2), 474–484.
- DNRM. (2016). Queensland's Petroleum and coal seam gas. In: *Mines*. CC15-GSQ104 Department of Natural Resources and Mines, Brisbane.
- Fu, G., Zhang, Y., & Zou, D. (1997). The measurement and analysis of the balanced contact angle between coal and pure water. *Coal Conversion*, *20*(4), 60–62. in Chinese.
- Fu, H. J., Tang, D. Z., Xu, H., Tao, S., Xu, T., Chen, B. L., & Yin, Z. Y. (2016). Abrupt changes in reservoir properties of low-rank coal and its control factors for methane adsorbability. *Energy and Fuels*, *30*, 2084–2094.
- Guo, H. J., Yuan, L., Cheng, Y. P., Wang, K., & Xu, C. (2019). Experimental investigation on coal pore and fracture characteristics based on fractal theory. *Powder Technology*, *346*, 341–349.
- Hamilton, S. K., Esterle, J. S., & Sliwa, R. (2014a). Stratigraphic and depositional framework of the Walloon Subgroup, eastern Surat Basin, Queensland. *Australian Journal of Earth Sciences*, *61*, 1061–1080.
- Hamilton, S. K., Golding, S. D., Baublys, K. A., & Esterle, J. S. (2014b). Stable isotopic and molecular composition of desorbed coal seam gases from the Walloon Subgroup, eastern Surat Basin, Australia. *International Journal of Coal Geology*, *122*, 21–36.
- Hamilton, S. K., Golding, S. D., Baublys, K. A., & Esterle, J. S. (2015). Conceptual exploration targeting for microbially en-

- hanced coal bed methane (MECoM) in the Walloon Subgroup, eastern Surat Basin, Australia. *International Journal of Coal Geology*, 138, 68–82.
- Han, L., Shen, J., Wang, J. Y., & Shabbiri, K. (2021). Characteristics of pore evolution and its maceral contributions in the Huolinhe lignite during coal pyrolysis. *Natural Resources Research*, 30, 2195–2210.
- Hodot, B. B. (1966). *Outburst of coal and coalbed gas*. China Industry Press. Chinese translation.
- Hou, S. H., Wang, X. M., Wang, X. J., Yuan, Y. D., Pan, S. D., & Wang, X. M. (2017). Pore structure characterization of low volatile bituminous coals with different particle size and tectonic deformation using low pressure gas adsorption. *International Journal of Coal Geology*, 183, 1–13.
- Howard, J. J., Kenyon, W. E., & Straley, C. (1993). Proton-magnetic resonance and pore-size variations in reservoir sandstones. *SPE Formation Evaluation*, 8, 194–200.
- ISO 11760-2005(E). (2005). Classification of coals.
- ISO 7404.3-1994. (1994). Methods for the petrographic analysis of bituminous coal and anthracite—Part 3: Method of determining maceral group composition.
- ISO 7404.5-1994. (1994). Method for the petrographic analysis of bituminous coal and anthracite—Part 5: Method of determining microscopically the reflectance of vitrinite.
- Jiu, B., Huang, W. H., & Hao, R. L. (2021). A method for judging depositional environment of coal reservoir based on coal facies parameters and rare earth element parameters. *Journal of Petroleum Science and Engineering*, 207, 109128.
- Kenyon, W. E., Day, P. I., Straley, C., & Willemsen, J. F. (1988). A three part study of NMR longitudinal relaxation properties of water-saturated sandstones. *SPE Formation Evaluation*, 3, 622–636.
- Laubach, S. E., Marrett, R. A., Olson, J. E., & Scott, A. R. (1998). Characteristics and origins of coal cleat: A review. *International Journal of Coal Geology*, 35, 175–207.
- Li, Y., Yang, J. H., Pan, Z. J., & Tong, W. S. (2020). Nanoscale pore structure and mechanical property analysis of coal: An insight combining AFM and SEM images. *Fuel*, 260, 116352.
- Li, Y., Zhang, C., Tang, D. Z., Gan, Q., Niu, X. L., Wang, K., & Shen, R. Y. (2017a). Coal pore size distributions controlled by the coalification process: an experimental study of coals from the Junggar, Ordos and Qinshui basins in China. *Fuel*, 206, 352–363.
- Li, Y. J., Zhai, C., Xu, J. Z., Yu, X., Sun, Y., Cong, Y. Z., Tang, W., & Zheng, Y. F. (2023). Effects of steam treatment on the internal moisture and physicochemical structure of coal and their implications for coalbed methane recovery. *Energy*, 270, 126866.
- Li, Z. T., Liu, D. M., Cai, Y. D., Ranjith, P. G., & Yao, Y. B. (2017b). Multi-scale quantitative characterization of 3-D pore-fracture networks in bituminous and anthracite coals using FIB-SEM tomography and X-ray  $\mu$ -CT. *Fuel*, 209, 43–53.
- Liu, P., Nie, B. S., Zhao, Z. D., Zhao, Y. L., & Li, Q. G. (2023). Characterization of ultrasonic induced damage on multi-scale pore/fracture in coal using gas sorption and  $\mu$ -CT 3D reconstruction. *Fuel*, 332, 126–178.
- Liu, S. Q., Wang, H., Wang, R., Gao, D. Y., & Tripathy, A. (2021). Research advances on characteristics of pores and fractures in coal seams. *Acta Sedimentologica Sinica*, 39, 212–230.
- Luo, Y. F., Xia, B. W., Li, H. L., Hu, H. R., Wu, M. Y., & Ji, K. N. (2021). Fractal permeability model for dual-porosity media embedded with natural tortuous fractures. *Fuel*, 295, 120610.
- Martin, M. A., Wakefield, M., MacPhail, M. K., Pearce, T., & Edwards, H. E. (2013). Sedimentology and stratigraphy of an intra-cratonic basin coal seam gas play: Walloon Subgroup of the Surat Basin, eastern Australia. *Petroleum Geoscience*, 19, 21–38.
- Mastalerz, M., & Drobniak, A. (2020). Coalbed Methane: Reserves, Production, and Future Outlook. In: *Future Energy* (3rd ed., pp. 97–109).
- Mohamed, T., & Mehana, M. (2020). Coalbed methane characterization and modeling: Review and outlook. *Energy Sources, Part A433A: Recovery, Utilization, and Environmental Effects+A465*. <https://doi.org/10.1080/15567036.2020.1845877>.
- Montgomery, S. L. (1999). Powder River Basin, Wyoming: An expanding coalbed methane (CBM) play. *AAPG Bulletin*, 83, 1207–1222.
- Moore, T. A. (2012). Coalbed methane: A review. *International Journal of Coal Geology*, 101, 36–81.
- Morris, J. R., & Martin, M. A. (2016). Coal architecture, high-resolution correlation and connectivity: New insights from the Walloon Subgroup in the Surat Basin of SE Queensland, Australia. *Petroleum Geoscience*, 23, 251–261.
- Mukherjee, S., Rajabi, M., Esterle, J., & Copley, J. (2020). Sub-surface fractures, in-situ stress and permeability variations in the Walloon Coal Measures, eastern Surat Basin, Queensland, Australia. *International Journal of Coal Geology*, 222, 103449.
- Nie, B. S., Liu, X. F., Yang, L. L., Meng, J. Q., & Li, X. C. (2015). Pore structure characterization of different rank coals using gas adsorption and scanning electron microscopy. *Fuel*, 158, 908–917.
- Ouyang, Z. Q., Liu, D. M., Cai, Y. D., & Yao, Y. B. (2016). Fractal analysis on heterogeneity of pore-fractures in middle-high rank coals with NMR. *Energy and Fuels*, 30(7), 5449–5458.
- Qin, Y., Moore, T. A., Shen, J., Yang, Z. B., Shen, Y. L., & Wang, G. (2018). Resources and geology of coalbed methane in China: A review. *International Geology Review*, 60, 777–812.
- Qu, J., Shen, J., Han, L., Ji, C. J., & Cheng, H. J. (2022). Characteristics of fractures in different macro-coal components in high-rank coal based on CT images. *Natural Gas Industry*, 42, 76–86.
- Queensland Government. (2018). *Petroleum and gas reserves statistics*. Available online: <https://www.data.qld.gov.au/data-set/petroleum-gas-production-and-reserve-statistics/resource/351e9bd4-d9a1-4d60-a2ed-0e56cae79c4a>.
- Queensland Government. (2019). *Petroleum and gas production statistics*. Available online: <https://www.data.qld.gov.au/data-set/petroleum-gas-production-and-reserve-statistics/resource/9746212a-e0c6-484d-95ad-b2be1c46027d>.
- Ramandi, H. L., Mostaghimi, P., Armstrong, R. T., Saadatfar, M., & Pinczewski, W. V. (2016). Porosity and permeability characterization of coal: A micro-computed tomography study. *International Journal of Coal Geology*, 154, 57–68.
- Salmachi, A., Rajabi, M., Wainman, C., Mackie, S., McCabe, P., Camac, B., & Clarkson, C. (2021). History, geology, in situ stress pattern, gas content and permeability of coal seam gas basins in Australia: A review. *Energies*, 14, 2651.
- Scott, S., Anderson, B., Crosdale, P., Dingwall, J., & Leblang, G. (2004). Revised geology and coal seam gas characteristics of the Walloon Subgroup—Surat Basin, Queensland. In P. J. Boulton, D. R. Johns, & S. C. Lang (Eds.), *Eastern Australasian basins symposium II* (pp. 345–355). Petroleum Exploration Society of Australia.
- Shen, J., Qin, Y., & Zhao, J. C. (2019). Maceral contribution to pore size distribution in anthracite in the south Qinshui Basin. *Energy and Fuels*, 33, 7234–7243.
- Shields, D., & Esterle, J. (2015). Regional insights into the sedimentary organisation of the Walloon Subgroup, Surat Basin, Queensland. *Australian Journal of Earth Sciences*, 62, 949–967.
- Su, X. B., Feng, Y. L., Chen, J. F., & Pan, J. N. (2001). The characteristics and origins of cleat in coal from Western North China. *International Journal of Coal Geology*, 47, 51–62.

- Sun, X. X., Yao, Y. B., Ripepi, N., & Liu, D. M. (2018). A novel method for gas–Water relative permeability measurement of coal using NMR relaxation. *Transport in Porous Media*, 124, 73–90.
- Tao, S., Chen, S. D., Tang, D. Z., Zhao, X., Xu, H., & Li, S. (2018). Material composition, pore structure and adsorption capacity of low-rank coals around the first coalification jump: A case of eastern Junggar Basin, China. *Fuel*, 211, 804–815.
- Thommes, M., Kaneko, K., Neimark, A. V., Olivier, J. P., Rodriguez-Reinoso, F., Rouquerol, J., & Sing, K. S. W. (2015). Physisorption of gases, with special reference to the evaluation of surface area and pore size distribution (IUPAC Technical Report). *Pure and Applied Chemistry*, 87, 1051–1069.
- Thompson, S., Morley, R. J., Barnard, P. C., & Cooper, B. S. (1985). Facies recognition of some Tertiary coals applied to prediction of oil source rock occurrence. *Marine and Petroleum Geology*, 2(4), 288–297.
- Wang, G., Shen, J. N., Liu, S. M., Jiang, C. H., & Qin, X. J. (2019). Three-dimensional modeling and analysis of macro-pore structure of coal using combined X-ray CT imaging and fractal theory. *International Journal of Rock Mechanics and Mining Sciences*, 123, 104082.
- Xin, F. D., Xu, H., Tang, D. Z., & Cao, C. (2022). Differences in accumulation patterns of low-rank coalbed methane in China under the control of the first coalification jump. *Fuel*, 324, 124657.
- Xu, J. Z., Zhai, C., Ranjith, P. G., Sang, S. X., Sun, Y., Cong, Y. Z., Tang, W., & Zheng, Y. F. (2022). Investigation of the mechanical damage of low rank coals under the impacts of cyclical liquid CO<sub>2</sub> for coalbed methane recovery. *Energy*, 239, 122145.
- Yao, Y. B., Liu, D. M., Cai, Y. D., & Li, J. Q. (2010a). Advanced characterization of pores and fractures in coals by nuclear magnetic resonance and X-ray computed tomography. *Science China: Earth Sciences*, 53, 854–862.
- Yao, Y. B., Liu, D. M., Che, Y., Tang, D. Z., Tang, S. H., & Huang, W. H. (2010b). Petrophysical characterization of coals by low-field nuclear magnetic resonance (NMR). *Fuel*, 89, 1371–1380.
- Yao, Y. B., Liu, D. M., Tang, D. Z., Tang, S. H., & Huang, W. H. (2008). Fractal characterization of adsorption-pores of coals from North China: An investigation on CH<sub>4</sub> adsorption capacity of coals. *International Journal of Coal Geology*, 73, 27–42.
- Yao, Y. B., Liu, D. M., Tang, D. Z., Tang, S. H., Huang, W. H., Liu, Z. H., & Che, Y. (2009). Fractal characterization of seepage-pores of coals from China: An investigation on permeability of coals. *Computers and Geosciences*, 35, 1159–1166.
- Zhang, C., Zhao, Y. S., Feng, Z. J., Meng, Q. R., Wang, L., & Lu, Y. (2023). Thermal maturity and chemical structure evolution of lump long-flame coal during superheated water vapor-based in situ pyrolysis. *Energy*, 263, 125863.
- Zhang, S. H., Tang, S. H., Tang, D. Z., Pan, Z. J., & Yang, J. (2010). The characteristics of coal reservoir pores and coal facies in Liulin district, Hedong coal field of China. *International Journal of Coal Geology*, 81, 117–127.
- Zhang, Z., Qin, Y., Zhuang, X. G., Li, G. Q., & Wang, X. M. (2018). Poroperm characteristics of high-rank coals from Southern Qinshui Basin by mercury intrusion, SEM-EDS, nuclear magnetic resonance and relative permeability analysis. *Journal of Natural Gas Science and Engineering*, 51, 116–128.
- Zhang, Z., Yan, D. T., Yang, S. G., Zhuang, X. G., Li, G. Q., Wang, G., & Wang, X. M. (2020). Experimental studies on the movable-water saturations of different-scale pores and relative permeability of low-medium rank coals from the Southern Junggar Basin. *Journal of Natural Gas Science and Engineering*, 83, 103585.
- Zhao, W., Wang, K., Liu, S. M., Ju, Y., Zhou, H. W., Fan, L., Yang, Y., Cheng, Y. P., & Zhang, X. L. (2020). Asynchronous difference in dynamic characteristics of adsorption swelling and mechanical compression of coal: Modeling and experiments. *International Journal of Rock Mechanics and Mining Sciences*, 135, 104498.
- Zhao, J. L., Xu, H., Tang, D. Z., Mathews, J. P., Li, S., & Tao, S. (2016a). Coal seam porosity and fracture heterogeneity of macrolithotypes in the Hancheng Block, eastern margin, Ordos Basin, China. *International Journal of Coal Geology*, 159, 18–29.
- Zhao, L., Qin, Y., Cai, C. F., Xie, Y. W., Wang, G., Huang, B., & Xu, C. L. (2016b). Control of coal facies to adsorption-desorption divergence of coals: A case from the Xiqu Drainage Area, Gujiao CBM Block, North China. *International Journal of Coal Geology*, 171, 169–184.
- Zhao, Y. X., Liu, S. M., Elsworth, D., Jiang, Y. D., & Zhu, J. (2014). Pore structure characterization of coal by synchrotron small-angle X-ray scattering and transmission electron microscopy. *Energy & Fuels*, 28, 3704–3711.
- Zheng, S. J., Yao, Y. B., Liu, D. M., Cai, Y. D., & Liu, Y. (2018). Characterizations of full-scale pore size distribution, porosity and permeability of coals: A novel methodology by nuclear magnetic resonance and fractal analysis theory. *International Journal of Coal Geology*, 196, 148–158.
- Zielar, L., Littke, R., & Schwarzbauer, J. (2018). Chemical and structural changes in vitrinites and megaspores from Carboniferous coals during maturation. *International Journal of Coal Geology*, 185, 91–102.
- Zou, C. N., Yang, Z., Huang, S. P., Ma, F., Sun, Q. P., Li, F. H., Pan, S. Q., & Tian, W. G. (2019). Resource types, formation, distribution and prospects of coal-measure gas. *Petroleum Exploration and Development*, 46(3), 451–462.

Springer Nature or its licensor (e.g. a society or other partner) holds exclusive rights to this article under a publishing agreement with the author(s) or other rightsholder(s); author self-archiving of the accepted manuscript version of this article is solely governed by the terms of such publishing agreement and applicable law.